Received: 16 November 2021 | Revised: 5 July 2022 | Accepted: 13 July 2022

DOI: 10.1111/bre.12703

Basin Research | IAS EAGE | WILEY

RESEARCH ARTICLE

Tectonic evolution of the Triassic Songpan-Ganzi basin as constrained by a synthesis of multi-proxy provenance data

Yan Tang[1,2] | **An Yin**[2] | **Xi Xu**[3,4] | **Kaixuan An**[4] | **Yunpeng Zhang**[5]

[1]School of Earth Science and Resources, Chang'an University, Xi'an, China

[2]Department of Earth, Planetary, and Space Sciences, University of California-Los Angeles, Los Angeles, California, USA

[3]China Aero Geophysical Survey and Remote Sensing Center for Natural Resources, China Geological Survey, Beijing, China

[4]School of Earth Sciences, Zhejiang University, Hangzhou, China

[5]Xi'an Center of China Geological Survey, Xi'an, China

Correspondence
An Yin, Department of Earth, Planetary, and Space Sciences, University of California-Los Angeles, Los Angeles, CA 90095-1567, USA.
Email: ayin54@gmail.com

Funding information
National Natural Science Foundation of China, Grant/Award Number: 41302047 and 41702044; Natural Science Foundation of Shaanxi Province, Grant/Award Number: 2018JM4003

Abstract

The triangular Songpan-Ganzi flysch terrane exposes a Triassic turbidite sequence with an average thickness of ca. 8 km. The sediments may have been accumulated in a remnant Paleo-Tethyan ocean bounded by the converging North China, South China, and the Qiangtang terrane from three sides, or a back-arc basin with an oceanic basement created during the Triassic closure of the Paleo-Tethyan ocean. To differentiate the two competing models, we systematically reviewed the available provenance data that include U–Pb detrital zircon ages at the basin scale, paleocurrent directions, sandstone petrography, and heavy-mineral assemblages from the Triassic Songpan-Ganzi basin samples. We use the Kolmogorov–Smirnov tests to differentiate competing hypotheses for detrital-zircon provenance interpretations and DZmix modelling to quantify relative contributions of detrital zircon from all potential source areas for the Triassic Songpan-Ganzi deposits. The most important result of this work is that the Songpan-Ganzi basin had a stable and locally derived source system: the western, central and eastern sub-basins were mainly sourced from the north whereas the easternmost and southeastern sub-basins were mainly sourced from westernmost South China (i.e., the Longmen Shan area) and the Qiangtang terrane. The stability of the source areas around the Songpan-Ganzi basin throughout the Triassic is most compatible with the remnant ocean model that predicts a long-lived marine basin with a pre-Triassic oceanic/continental basement trapped between converging continental blocks during the Triassic.

1 | INTRODUCTION

The triangular Triassic Songpan-Ganzi flysch basin is bounded by the Kunlun-Qaidam terrane and North China block (NCB) to the north, the Qiangtang terrane and Yidun arc terrane to the south, and the South China block (SCB) strongly modified by the Cenozoic Longmen Shan thrust belt to the east (Figure 1) (Burchfiel & Chen, 2012). The Songpan-Ganzi basin is composed dominantly of Triassic submarine-fan deposits with an estimated average thickness of ca. 8 km over an area of >370,000 km^2 (Nie et al., 1994; Pan et al., 2004; Yin & Nie, 1993, 1996). Although the formation of this basin has been considered as a result of the final Late Triassic closure of the Paleo-Tethyan ocean (Sengör, 1984; Stampfli & Borel, 2002; Weislogel, 2008) (Figure 1), the source of basin deposits and exact tectonic processes responsible for the sediment accumulation remains debated. In the current literature,

all the surrounding orogenic belts, cratons, and arc terranes have been variably considered as potential source areas under variously inferred tectonic settings (e.g., Bruguier et al., 1997; Chang, 2000; Ding et al., 2013; Enkelmann et al., 2007; Jian et al., 2019; Nie et al., 1994; Roger et al., 2008, 2010; She et al., 2006; Tang et al., 2017, 2018; Wang et al., 2007; Weislogel, 2008; Weislogel et al., 2006, 2010; Zhang, Tang, et al., 2014; Zhang, Zeng, et al., 2015; Zhou & Graham, 1996).

In the eastern part of the Songpan-Ganzi basin (i.e., eastern domain in Figure 1), Weislogel et al. (2010) showed that Triassic strata were accumulated in three subsidiary depocentres, each having distinct sediment sources. Weislogel et al. (2010) conclude that the northern and central subsidiary depocentres were mainly sourced from North China and the Triassic Qinling-Dabie orogeny between North and South China. The above conclusion is consistent with the remnant ocean basin model of Nie et al. (1994) and Zhou and Graham (1996) that requires the Songpan-Ganzi basin to have been sandwiched between the coevally evolving Qinling-Dabie collisional orogen and the impinging Yidun arc and Qiangtang terrain in the north, west and south, respectively. Weislogel et al. (2010) also demonstrate that the southeastern subsidiary depocentre was sourced from South China and the

Highlights

1. The Songpan-Ganzi basin is consistent with the remnant ocean model, which requires its basement to be part of South China.
2. The easternmost Songpan-Ganzi basin was sourced from the western South China margin.
3. DZmix modelling of the Songpan-Ganzi detrital-zircon age data supports the remnant ocean model.

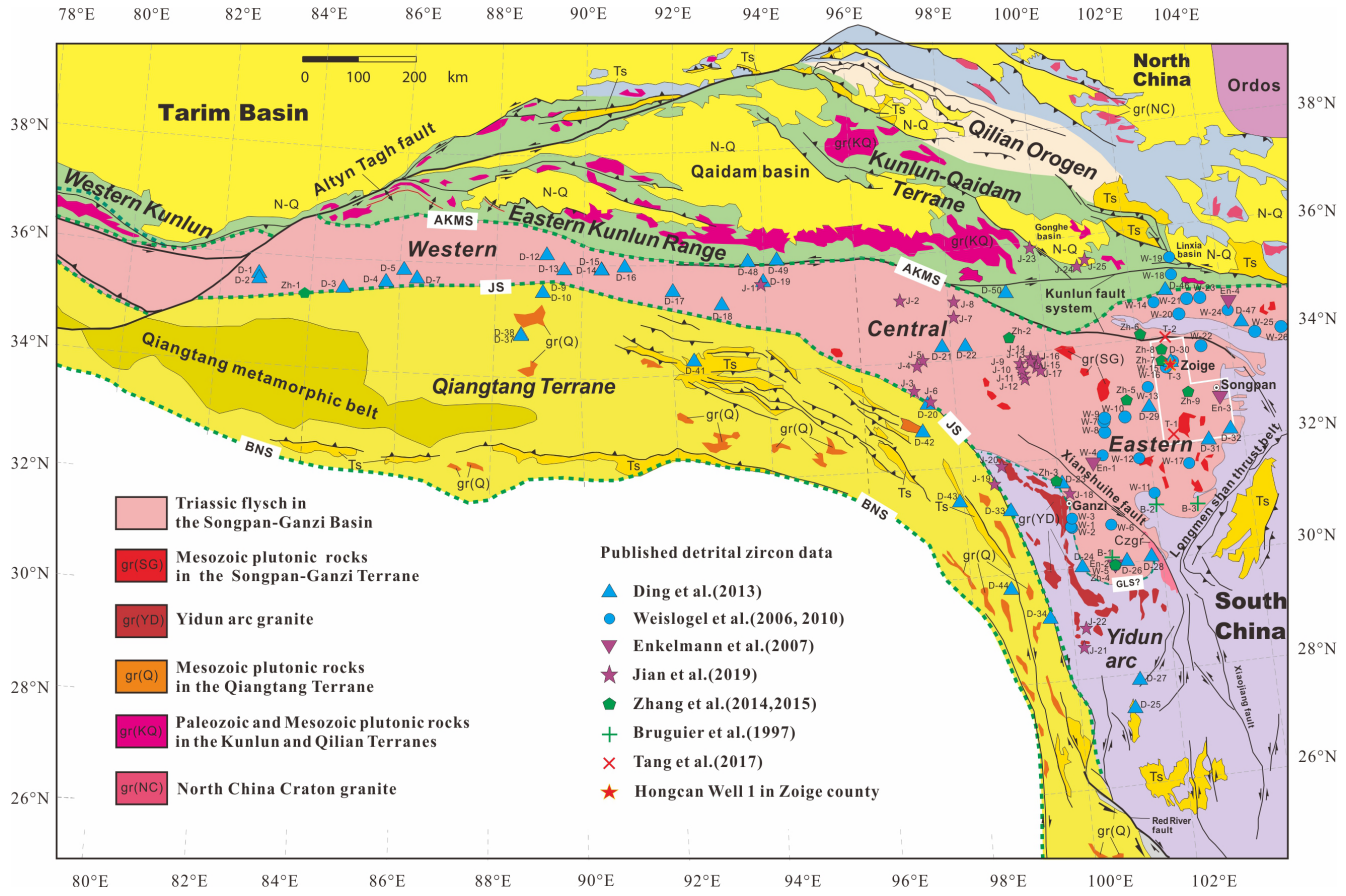

FIGURE 1 Tectonic map showing the Songpan-Ganzi basin and surrounding major terranes, suture zones and published sample locations (Table S1) in the northern part of the Tibetan plateau. Map compiled after Yin and Harrison (2000) and Wu et al. (2016). This study area located in the Zoige and Songpan County marked with a white rectangle (enlarged in Figure 18). Major plutonic rocks: Czgr, Cenozoic granites in eastern Tibet; gr(KQ), Palaeozoic and Mesozoic plutonic rocks in the Kunlun and Qaidam terranes; gr(NC), North China craton granite; gr(Q), Mesozoic plutonic rocks in the Qiangtang terrane; gr(SG), Mesozoic plutonic rocks in the Hoh-Xil-Songpan-Ganzi terrane; gr(YD), Yidun arc granite; major sutures: AKMS, Anyimaqen-Kunlun-Mianlue suture; BNS, Bangong-Nujiang suture; JS, Jinsha suture.

Yidun arc, possibly resulting from an oblique collision between the Yidun terrane and South China.

In the western part of the Songpan-Ganzi basin (i.e., western domain in Figure 1), Ding et al. (2013) use detrital zircon ages as provenance proxies and show that the Triassic sediments there were most likely sourced from North China, South China, the Qiangtang terrane and the Kunlun batholith belt along the southern margin of the Kunlun-Qaidam terrane. These authors suggest that detritus derived from the distal sources such as South China and western North China was transported to the western Songpan-Ganzi basin by a >1500-km fluvial and submarine transport system. Ding et al. (2013) envision that the basin in-filling occurred during the final closure of the eastern Paleo-Tethyan ocean, a scenario generally similar to the earlier suggestions of Sengör (1984), Stampfli and Borel (2002) and Weislogel (2008). A key difference between Ding et al.'s (2013) interpretations and those of earlier studies by Sengör (1984), Stampfli and Borel (2002) and Weislogel (2008) is that they envision the Paleo-Tethyan crust was extended and thinned during the Triassic Tethyan-ocean closure by a slab roll-back process, which resulted in the separation of the Yidun arc terrane from the southern margin of the Kunlun-Qaidam terrane. The model of Ding et al. (2013) follows the earlier proposed Mediterranean-style model of Pullen et al. (2008) for the Triassic development of the Songpan-Ganzi basin.

In the central part of the Songpan-Ganzi basin (i.e., central domain in Figure 1), Jian et al. (2019) use detrital zircon ages as provenance proxies and show that the Triassic strata in the area were largely derived from the southern margin of the Kunlun-Qaidam terrane and North China from the north. They also find that Triassic sediments of the southern Songpan-Ganzi basin and Yidun terrane were mainly derived from the basement of the Yidun arc and the Jinsha suture zone. Jian et al. (2019) conclude that their detrital-zircon-age data are most consistent with the remnant-ocean-basin model of Nie et al. (1994) and Zhou and Graham (1996) rather than the Mediterranean-style model of Pullen et al. (2008) and Ding et al. (2013). The above two competing tectonic models for the development of the Songpan-Ganzi turbidite basin make distinctively different first-order predictions. The remnant ocean model predicts that the basin floor is either oceanic or continental, both belonging to the western continuation of the South China lithosphere; the model also requires that the Yidun arc basement is the same as that of South China (Weislogel, 2008; Weislogel et al., 2006, 2010). In contrast, the back-arc extension model predicts the basin floor to be either extremely attenuated basement of the Kunlun-Qaidam terrain or a latest Triassic oceanic crust; the Yidun arc basement correlates with the basement of the Kunlun-Qaidam terrane. Note that the remnant-ocean model does not require the existence of an oceanic crust on the west side of South China. As argued in Wu et al. (2016), the basement of the Songpan-Ganzi basin may be entirely continental and is part of the thinned continental crust of South China.

A critical issue with the existing studies on the origin and sedimentary history of the Triassic Songpan-Ganzi basin is that individual studies emphasize strongly the effect of boundary conditions near the study areas, but a lack of systematic and holistic integration and analysis of all existing data limit the ability of early studies to explore all possible interpretations. In addition, heavy-mineral assemblages, which are additional proxies for finger-printing source rocks, have not been integrated with the early provenance analysis using sedimentological and detrital-zircon geochronological data. Finally, statistically based quantitative provenance analysis has not yet been applied to the existing Songpan-Ganzi Triassic U–Pb detrital-zircon age data set. To address the above issues, we present a state-of-the-art synthesis of all relevant data for a basin-scale provenance reconstruction. The data used in this study are mostly from the existing literature except heavy-mineral analysis exclusively from our work. Quantitative modelling of the detrital-zircon age data in particular permits a coherent interpretation of the Songpan-Ganzi basin evolution in the context of testing the two competing tectonic models mentioned above. The results of this synthesis show that the provenance of the Songpan-Ganzi basin is most consistent with the remnant ocean model.

2 | GEOLOGIC SETTING

The Songpan-Ganzi basin coincides with the Songpan-Ganzi terrane that is best exposed in the Cenozoic Tibetan plateau between the Kunlun and Jinsha suture zones in the north and south and South China in the east (Figure 1). Triassic strata are also exposed in the basin-bounding regions such as the southern Kunlun Shan region of the Kunlun-Qaidam terrane, the northern Qiangtang terrane, Yidun arc, western Qinling orogen and the Sichuan Basin of South China (Figure 2). The Triassic strata in the Songpan-Ganzi basin can be divided into the western sector consisting of the Bayan Har Group and the eastern sector consisting of the Xikang Group that includes Zagunao, Zhuwo and Xinduqiao Formations, respectively (Figure 2) (BGMRQP, 1991). These units are dominated by shales, siltstones, sandstones and minor carbonates (BGMRSP, 1991). The Precambrian crystalline basement and the base of the Triassic strata are exposed in the eastern sector of the Songpan-Ganzi basin, where Triassic sediments rest conformably on top of Permian strata and disconformably on top of Devonian strata (Wang, Pan, et al., 2013; Wu et al., 2016).

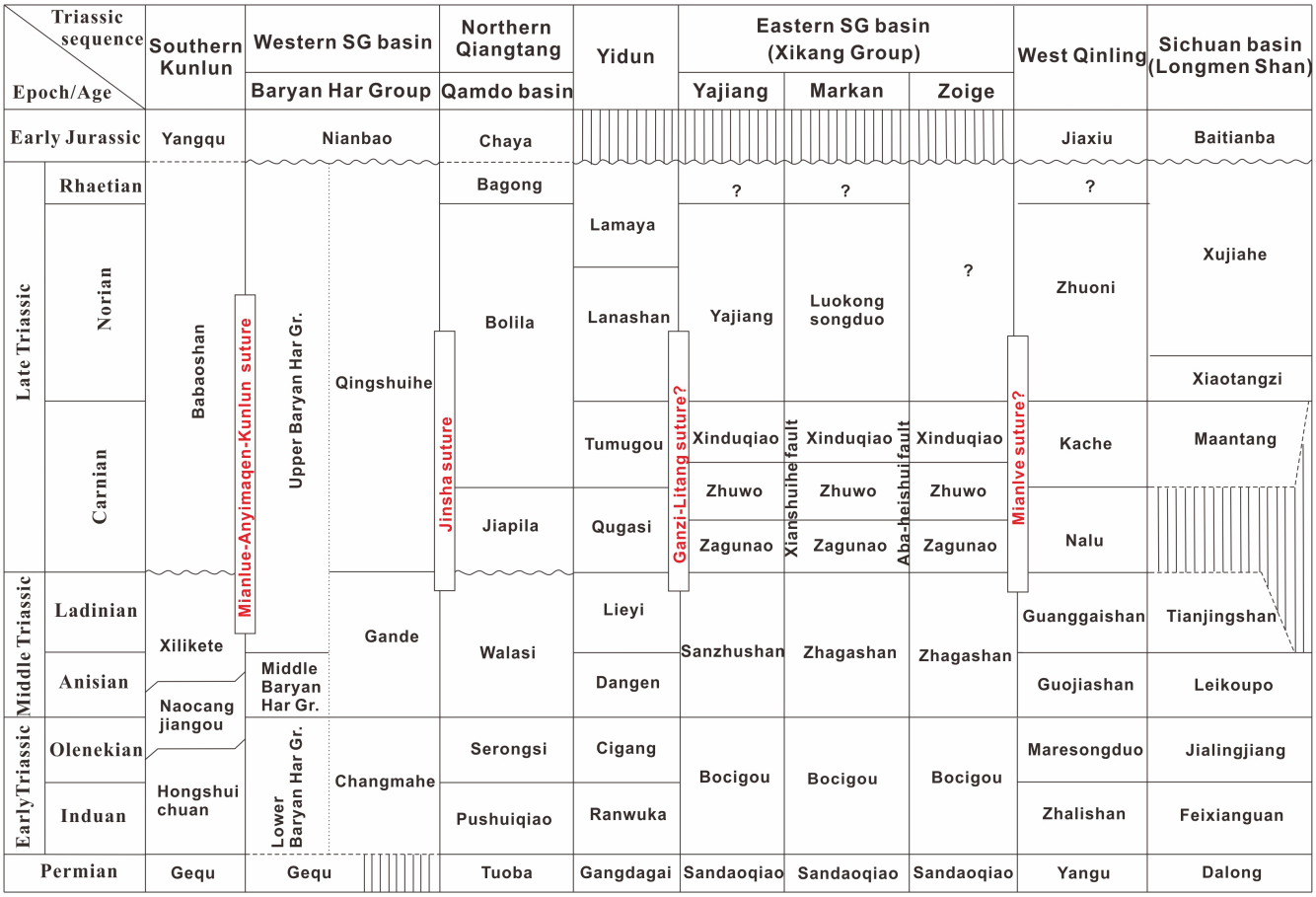

FIGURE 2 Triassic sequence system in the Songpan-Ganzi basin and its surroundings, such as southern Kunlun, northern Qiangtang, Yidun, west Qinling and Sichuan basin for comparison. Figure is after BGMRQP (1991), BGMRSP (1991) and Yang et al. (2000).

Regional tectonic analysis shows that the Paleo-Tethyan oceanic lithosphere was subducting northward beneath the southern margin of Asia composed of North China and the Kunlun-Qaidam terrane along the Mianlue-Anyimaqen-Kunlun suture from the Late Devonian to the Early Permian (Matte et al., 1996; Ratschbacher et al., 2006; Roger et al., 2011). By Early Triassic time, the Paleo-Tethyan oceanic lithosphere was also subducting southward beneath the Qiangtang terrane along the Jinsha suture (Dewey et al., 1988; Roger et al., 2010). Closure of the Paleo-Tethyan ocean and the subsequent collision between North China and South China may have occurred diachronously along strike, starting in the east during the Early Triassic and possibly the latest Permian that resulted in the Qinling-Dabie orogen and high-pressure to ultrahigh-pressure metamorphism (e.g., Hacker et al., 2006; Liou et al., 2000; Yin & Nie, 1993, 1996). Westward progression of the ocean closure is manifested by the final consumption of the Paleo-Tethyan oceanic lithosphere between the Kunlun-Qaidam and Qiangtang terranes in the Latest Triassic and possibly earliest Jurassic time (Dewey et al., 1988; Ding et al., 2013; Roger et al., 2004; 2010; Sengör, 1984; Yin & Harrison, 2000).

The Triassic Songpan-Ganzi basin was widely intruded by Late Triassic to Early Jurassic plutons, best expressed in the eastern part of the basin (Figure 3a) (e.g., Roger et al., 2004; Xiao et al., 2007; Yuan et al., 2010; Zhang et al., 2006, 2007; Zhang, Ding, et al., 2014). It is worth noting that many of these granitoids were emplaced during ongoing deep-marine sedimentation, and they exhibit a wide range of compositions that can be characterized as adakites, and I-, A- and S-type granites (Figure 3b) (Roger et al., 2004; Xiao et al., 2007; Yuan et al., 2010; Zhang et al., 2006, 2007; Zhang, Ding, et al., 2014). The origin of the Triassic magmatism is variably attributed to (1) partial melting of the thickened Songpan-Ganzi sedimentary cover and a basement equivalent to the Yangtze craton (Roger et al., 2004), (2) partial melting of both the asthenospheric mantle and the lower continental crust in response to lithospheric mantle delamination (Xiao et al., 2007; Yuan et al., 2010; Zhang et al., 2006, 2007), (3) partial melting of both the Paleo-Tethyan oceanic slab and overlying continental arc induced by slab rollback (Zhang, Ding, et al., 2014), and (4) double-slab retreat (De Sigoyer et al., 2014).

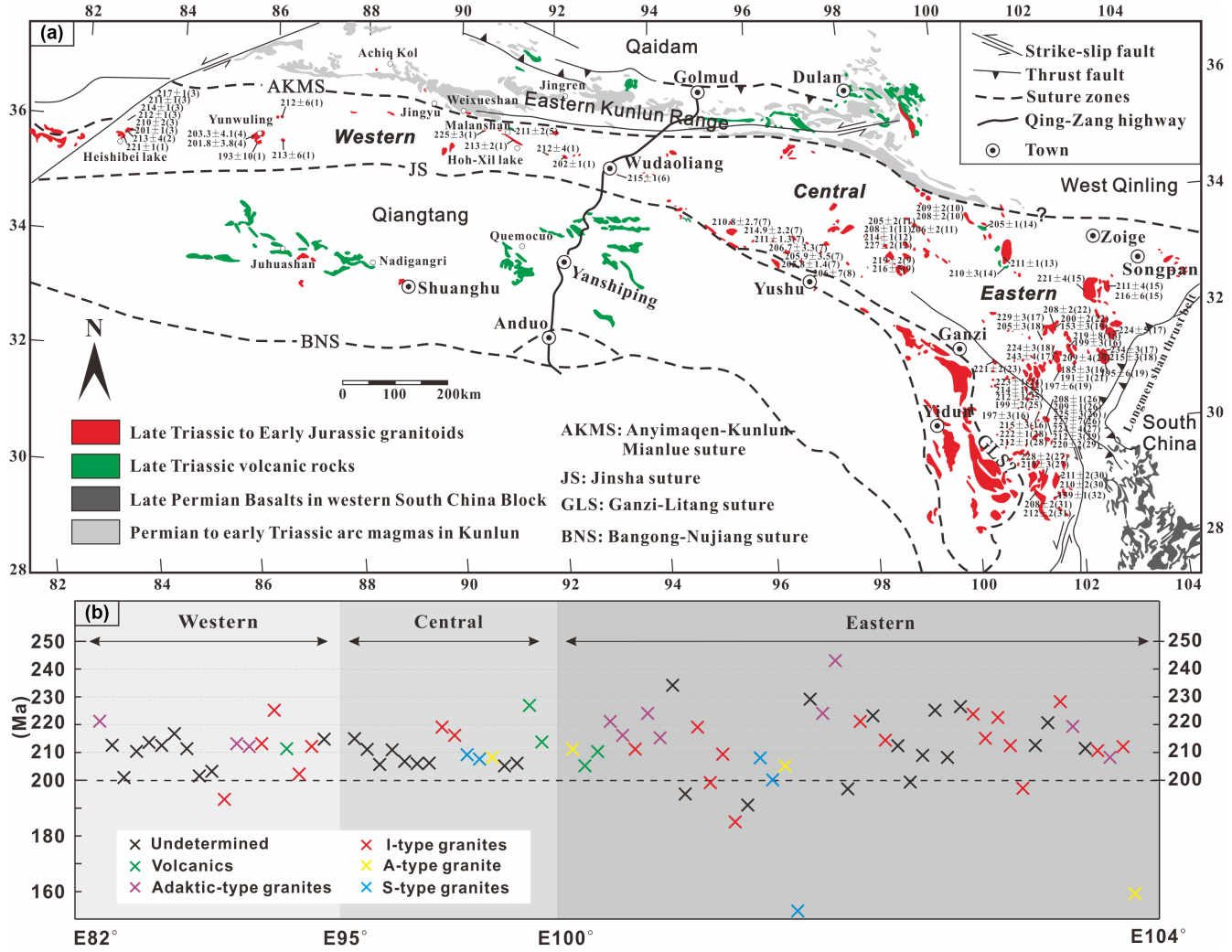

FIGURE 3 Spatial and temporal distributions of plutons in the Songpan-Ganzi basin. (a) Is for plane view (revised after Wang et al. (2018) and Zhang, Ding, et al. (2014)); (b) is for section view. Age data are cited and listed in Table S2.

3 | AGE CHARACTERIZATION OF THE BASIN-BOUNDING TERRANES

In order to constrain the provenance of the Triassic Songpan-Ganzi deposits, we tabulate three types of age data: (1) zircon ages of pre-Triassic metamorphic basement rocks (i.e., Figure 4a–f), (2) detrital-zircon ages of Triassic strata in regions bounding the Songpan-Ganzi basin (i.e., Figure 4a–f), and (3) U–Pb zircon ages of Phanerozoic plutonic rocks (Figure 5a–c).

3.1 | North China

U–Pb zircon dating of North China basement rocks (Darby & Gehrels, 2006; Hu et al., 2009; Tung et al., 2007; Xia, Sun, Zhao, & Luo, 2006; Xia, Sun, Zhao, Wu, et al., 2006), which are dominantly metasedimentary and metavolcanic rocks, shows a general bimodal-age distribution centred at 1.88 and 2.5 Ga, respectively, and a noticeable lack of significant Neoproterozoic ages (Figure 4a) (Table S3). The detrital zircon ages of Triassic non-marine clastic rocks in the Ordos area (Figure 1) of western North China (Figure 4a) (Table S4) (Weislogel et al., 2010; Yang et al., 2014) are similar to the detrital zircon age distribution of the Triassic marine turbidite in the western Qinling area (Figure 4b) (Table S4) (Ding et al., 2013; Jian et al., 2019; Weislogel et al., 2010) (i.e., two prominent peaks at ca. 2.5 and 1.87 Ga, an absence of 1000–800 Ma grains, and an age cluster of 250–275 Ma). Note that the western Qinling turbidite yields a dominant age peak at ca. 445 Ma, whereas Triassic strata of North China only have a few ca. 360 Ma grains.

3.2 | Qinling orogen

Metamorphic basement rocks of the North Qinling terrane (Figure 4b) (Table S3) (Diwu et al., 2010, 2014; Lu

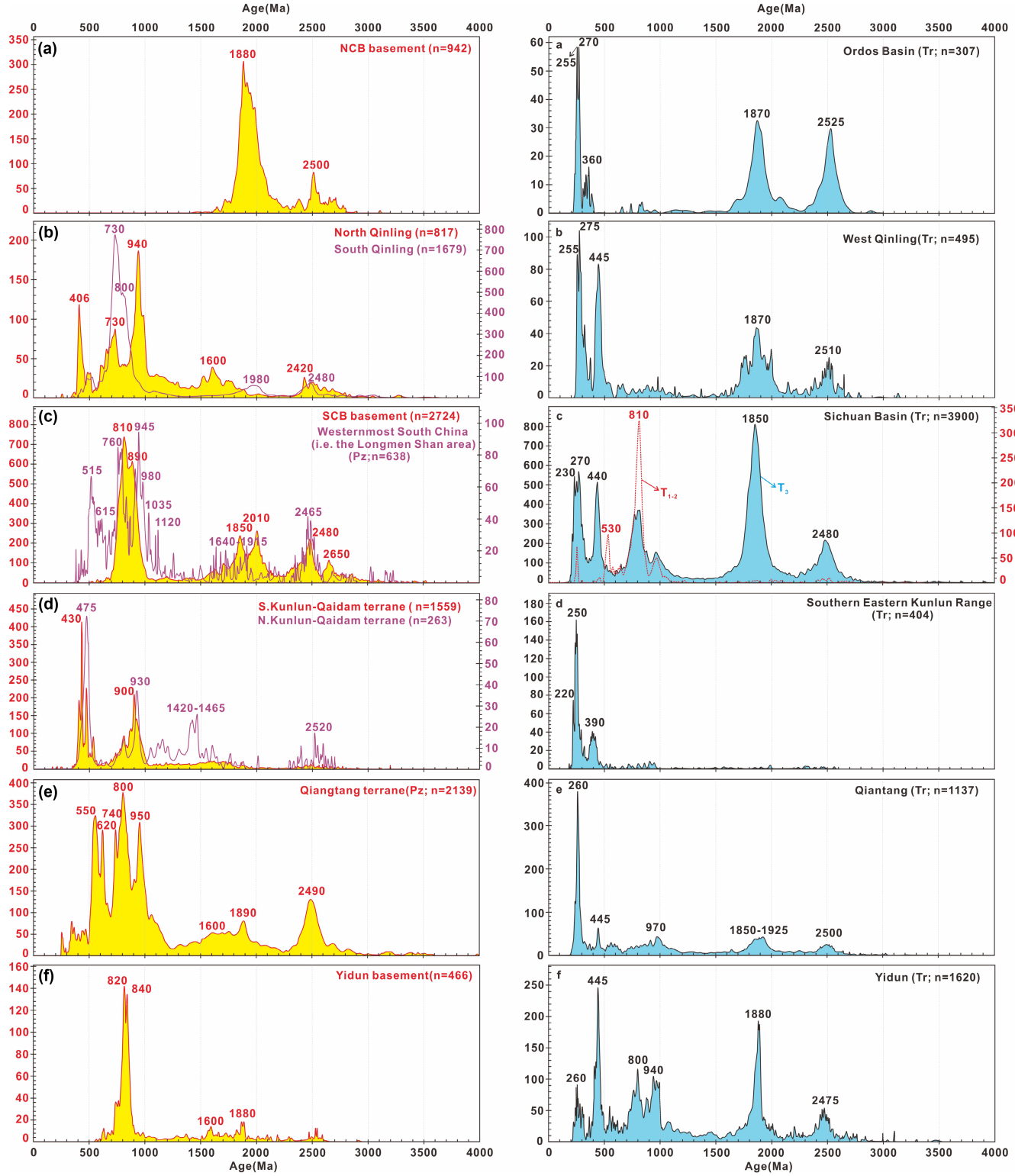

FIGURE 4 Zircon signatures of pre-Triassic metamorphic basement rocks (left; Figure 4a–f) and detrital-zircon ages of Triassic strata in regions bounding the Songpan-Ganzi basin (right; Figure 4a–f). Age data are cited and listed in Tables S3 and S4 in details.

et al., 2006; Shi et al., 2009, 2013; Wan et al., 2011; Zhu et al., 2011) yield three major age peaks at ca. 730, 940, and 1600 Ma, and a minor age cluster at 2.4–2.5 Ga. Metamorphic basement rocks of the South Qinling terrane (Figure 4b) (Table S3) (e.g., Dong et al., 2013; Ling et al., 2010; Liu & Zhang, 2013; Shi et al., 2013; Wang, Griffin, et al., 2013; Yan et al., 2003; Zhu et al., 2014) are characterized by a significant Neoproterozoic age cluster at 730–800 Ma, and minor age clusters at ca. 2.0 and 2.5 Ga, respectively. The North and South Qinling terranes differ (Figure 5a) (Table S5) in

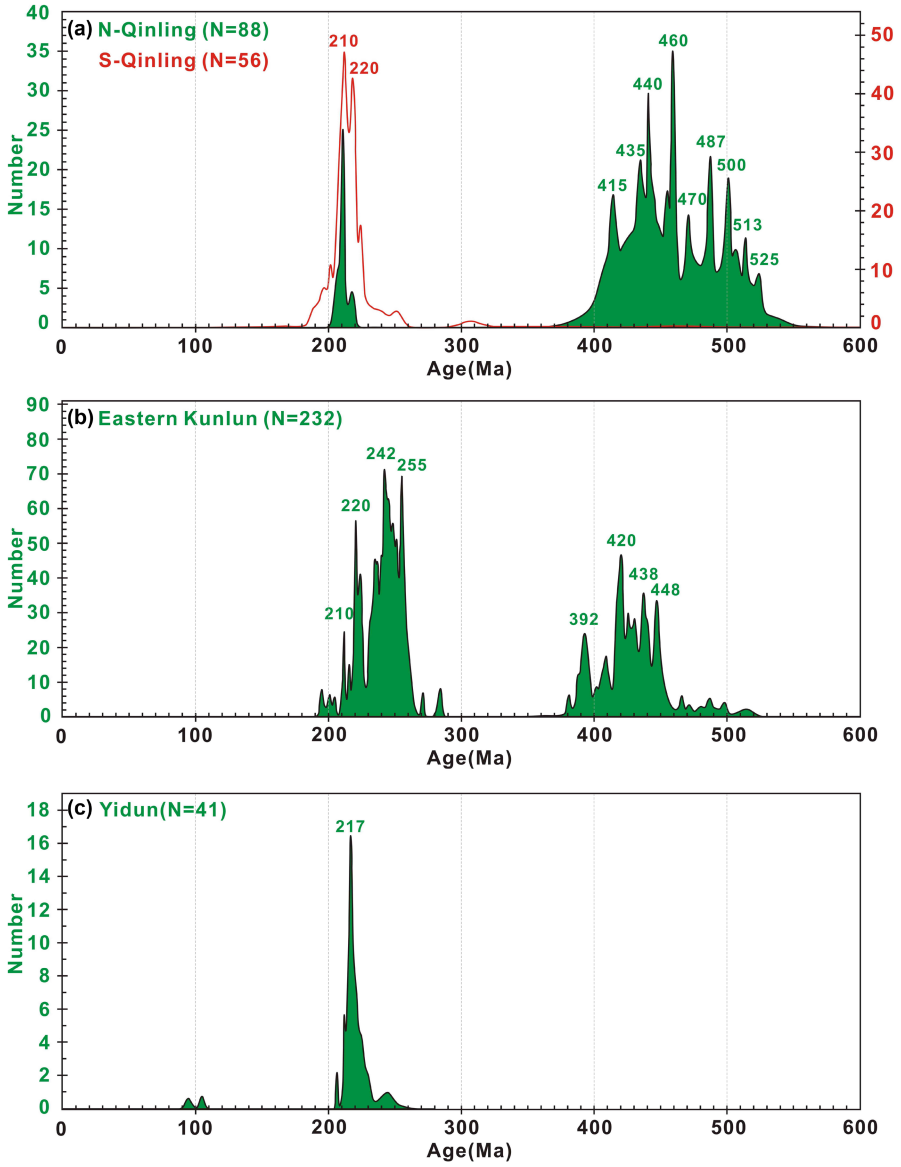

FIGURE 5 Relative probability plots of U–pb zircon ages of phanerozoic plutonic rocks in: Qinling orogen (a), eastern Kunlun range (b) and Yidun terrane (c). Age data are cited and listed in Table S5 in details.

that the North Qinling terrane (e.g., Dong et al., 2011; Jiang et al., 2009; Lerch et al., 1995; Lu et al., 2003; Pei, Ding, Li, et al., 2007; Pei, Ding, Zhang, et al., 2007; Wang, Wang, et al., 2011; Xue et al., 1996; Yan et al., 2007, 2008) experienced magmatism in the Early Palaeozoic (525–415 Ma) and the Late Triassic (220–210 Ma) whereas the South Qinling terrane (e.g., Dong et al., 2012; Gong et al., 2009; Jiang et al., 2010; Jin et al., 2005; Qin et al., 2007, 2008, 2009; Sun et al., 2000) experienced only the Late Triassic magmatism.

3.3 | South China

The basement of South China (Figure 4c) (Table S3) (Chen et al., 2013; Liu et al., 2008; Sun & Zhou, 2008, 2009; Wang, Griffin, et al., 2010, 2013; Wang, Zhou, et al., 2007; Wang, Yu, et al., 2012) has a dominant age cluster at ca. 810–890 Ma, a prominent age cluster at ca. 1.8–2.0 Ga and a minor age population at ca. 2.6–2.4 Ga. Detrital zircon dating of Palaeozoic sedimentary strata of westernmost South China exposed in the Cenozoic Longmen Shan thrust belt (Figure 4c) (Table S3) (Chen et al., 2016; Duan et al., 2011; Jian et al., 2019; Weislogel et al., 2010) yields a major population at 760–950 Ma, significant Pan-African (510–610 Ma) and some Grenville (980–1120 Ma) zircon ages, and minor populations of Paleoproterozoic (1.6–1.9 Ga) and Archean (ca. 2.5 Ga) zircon ages.

Detrital zircon dating of Upper Triassic samples (e.g., the Xujiahe Formation) from the Sichuan Basin of South China (Figure 4c) (Table S4) (e.g., Shao et al., 2016; Weislogel et al., 2010; Yan et al., 2018; Zhang, Jia, et al., 2015; Zhu et al., 2017) shows major age clusters at ca. 1.85 Ga, 270–230 Ma and 440 Ma, and minor age peaks at ca. 2.5 Ga and 820–770 Ma. This age distribution differs markedly from that of the Middle to Lower Triassic strata in the same area that displays a significant Neoproterozoic peak age at

ca. 810 Ma, a dearth of Paleoproterozoic and Archean zircon ages, and two minor peaks at ca. 250 and 530 Ma (Yan et al., 2018; Zhu et al., 2017) (Figure 4c) (Table S4).

3.4 | Kunlun-Qaidam terrane

The Eastern Kunlun Range basement in the southern margin of the Kunlun-Qaidam terrane (Figure 4d) (Table S3) (e.g., He et al., 2016; Jian et al., 2020; Meng et al., 2017; Wu et al., 2016) exposes Neoproterozoic plutons with ages at ca. 900 Ma. Similarly, the northern margin of the Kunlun-Qaidam terrane (i.e., the combined 'North Qaidam' and 'Qilian orogen' in Gehrels et al., 2003) exposes Neoproterozoic plutons with ages mostly centred at ca. 930 Ma. Metasedimentary basement rocks in the two regions yield detrital zircon ages clustered at 1.4–1.5 Ga and ca. 2.5 Ga (Figure 4d) (Table S3).

Zircon ages of Phanerozoic igneous rocks from the Eastern Kunlun Range (Figure 5b) (Table S5) (e.g., Chen et al., 2012; Dai et al., 2013; Ding et al., 2014, 2015; He et al., 2018; Li et al., 2013, 2015, 2018; Qi, 2015; Shao et al., 2017; Wu et al., 2016; Xiong et al., 2013, 2014, 2015, 2016, 2019; Zhang et al., 2012; Zhou et al., 2020) show two episodes of arc magmatism at 448–392 and 255–210 Ma, respectively. These ages overlap with detrital zircon ages obtained from the southern Eastern Kunlun Triassic strata (Figure 4d) (Ding et al., 2013; Wu et al., 2016) that show two prominent age peaks centred at ca. 390 Ma (with a range of 420–380 Ma) and ca. 250 Ma (with a range of 255–220 Ma). These ages correlation suggests that the Kunlun Triassic strata were sourced from the local Eastern Kunlun batholith belt.

3.5 | Qiangtang terrane

Detrital zircon ages from the Palaeozoic strata in the Qiangtang terrane (Figure 4e) (Table S3) (Gehrels et al., 2011; He et al., 2011; Pullen et al., 2008, 2011) are dominated by two clusters at 740–950 and 550–620 Ma, along with a two minor populations of Paleoproterozoic and Archean zircon ages at 1.6–1.9 and 2.5 Ga. Zircon ages from the Triassic strata exposed in the Qiangtang terrane show a major peak at ca. 260 Ma and several minor age peaks at ca. 2.5, 1.9, 970, 445 Ma, respectively (Figure 4e) (Table S4) (Ding et al., 2013; Gehrels et al., 2011).

3.6 | Yidun arc terrane

Detrital zircon dating of the Yidun arc basement rocks (Figure 4f) (Table S3) (Jian et al., 2019; Su et al., 2019) shows an age peak at ca. 810 Ma and a minor population of 1.6–1.88 Ga zircon ages. Zircon ages from the Triassic Yidun strata (Figure 4f) (Table S4) (Ding et al., 2013; Jian et al., 2019; Wang, Wang, et al., 2013) yield peaks and clusters at ca. 2.5 Ga, 1.88 Ga, 800–940 Ma, 445 Ma and 260 Ma, respectively. U–Pb zircon dating of dioritic–granitic plutons in the Yidun arc (e.g., Leng et al., 2012; Liu et al., 2006; Peng et al., 2014; Reid et al., 2007; Wang, Zhou, et al., 2011; Weislogel, 2008) shows a predominant age peak at ca. 217 Ma (Figures 3 and 5c) (Table S5).

4 | DATA AND METHODS

4.1 | Detrital zircon geochronology

Detrital zircon geochronology is a powerful method to assess sedimentary provenances. Early interpretations of detrital age distributions relied on qualitative comparison based on the presence or absence of characteristic source populations for a given geologic setting, often highlighted by vertical bars on vertically stacked finite mixture distributions. More recently, quantitative techniques have been adapted to aid comparison of detrital data sets, but there is no widely accepted method of unmixing detrital geochronology age distributions. Sundell and Saylor (2017) developed DZmix method, which is designed to quantify source-mixing proportions through a combination of inverse Monte–Carlo modelling and optimized forward modelling, so as to obtain the relative contribution of source areas. A software for DZmix analysis used in this study is available at https://github.com/kurtsundell/DZmix.

A total of 6483 U–Pb detrital zircon ages of 84 Triassic samples from the Songpan-Ganzi basin have been reported in the existing literature, which are selected for our DZmix analysis. Following Sundell and Saylor (2017), we regard the Triassic Songpan-Ganzi detrital zircon age data as a mixed population from several potential source areas, and randomly simulate among them that yield the best matching models. Model results generated using the KS D statistics, Kuiper V statistics and cross-correlation coefficients (R^2) are reported as the mean and one standard deviation of the best 100 model fits that have the lowest D and V values and the highest R^2 values out of 10,000 model trials.

4.2 | Paleocurrent direction data

Paleocurrent orientation data are compiled from the western, central and eastern Songpan-Ganzi Triassic strata collected by Weislogel et al. (2010), Ding et al. (2013) and Jian et al. (2019). This yields a total of 962 paleocurrent-orientation data at 57 locations. Paleocurrent orientations were primarily

determined from flute casts, ripple casts and ripple foresets, as well as tool marks and groove casts. Measurements were corrected for horizontal bedding rotations. Paleomagnetic studies indicate negligible vertical axis rotations in the majority of the northern Tibetan plateau in the Cenozoic (e.g., Dupont-Nivet et al., 2002; Halim et al., 1998).

4.3 | Petrology

Traditional Gazzi-Dickinson point counting of at least 300 relevant grains of quartz, feldspar and lithic rock fragments (>0.0625 mm) was undertaken to acquire light mineral modes used to produce ternary plots (Dickinson et al., 1983). The fields in the diagrams for QFL (quartz-feldspar-lithics) and QmFLt (quartz monocrystalline-feldspar-lithic total) have been widely interpreted to indicate possible derivation from 'continental block', 'recycled orogen' or 'magmatic arc' settings.

A total of 50 Triassic sandstones from the eastern Songpan-Ganzi basin (see the study area in Figure 1) were selected for detailed petrographic observations. We use the compositional area method to estimate the content of detrital components with an error of <5%. Some frame grains in the sandstone samples are modified by late diagenesis, which does not alter the morphology of the grain and our point-count results.

4.4 | Heavy mineral

A total of 44 Triassic sandstones from the eastern Songpan-Ganzi basin (see the study area in Figure 1) were selected for heavy mineral analysis. This work was conducted in the Chengxin Geology Service Co. Ltd, Langfang, Hebei Province, China. All samples were crushed, sieved, washed and then separated using magnetic and electromagnetic methods. The identification of the heavy minerals was performed manually using a binocular microscope. Each sample weighs ≥2 kg and ca. 1000 grains from each sample were analysed. The percentage of heavy minerals was calculated based on the weight.

5 | RESULTS

5.1 | Detrital zircon ages of the Triassic Songpan-Ganzi strata

5.1.1 | Spatial distributions of detrital-zircon ages

We tabulate a total of 6483 U–Pb detrital zircon ages from 84 samples from the Songpan-Ganzi basin that are reported in the existing literature. In order to better compare and/or contrast among these samples, we divide the Songpan-Ganzi basin into five domains: (1) the western domain between 82°E and 95°E, (2) the central domain between 95°E and 100°E, (3) the eastern domain between 100°E and 105°E, (4) the northeastern domain along the northeastern basin margin, and (5) the southeastern domain along the southeastern basin margin (Figure 6a) (Table S6) (Bruguier et al., 1997; Ding et al., 2013; Enkelmann et al., 2007; Jian et al., 2019; Tang et al., 2017; Wang, Li, et al., 2007; Weislogel et al., 2006, 2010; Zhang, Tang, et al., 2014; Zhang, Zeng, et al., 2015).

Western domain (Figure 6b)

The detrital zircon ages in this domain displays major age peaks at 242–263 and 432–442 Ma, and minor age clusters at 774–959 Ma, ca. 1.9, and 2.5 Ga. Late Triassic samples yield more detrital zircon grains with ages at ca. 1.9 Ga than those from the Early and Middle Triassic samples.

Central domain (Figure 6c)

The detrital zircon ages from Early Triassic show peaks at 265–300 and 450 Ma along with a dearth of Precambrian zircon ages. The zircon ages from the Middle Triassic strata show major age peaks at 250–300, 426–495 Ma and ca. 1.87 Ga and minor age clusters at 758–935 Ma and ca. 2.5 Ga. The zircon ages from the Late Triassic samples show similar Phanerozoic zircon age peaks to those from the Early and Middle Triassic samples at 250–300 and 426–495 Ma; however, they yield relatively fewer Precambrian zircon age peaks and lusters at 768–916 Ma, ca. 1.9, and 2.5 Ga.

Eastern domain (Figure 6d)

The detrital zircon ages from Early Triassic samples display an age spectrum with peaks at ca. 760 Ma (with a range from 700 to 850 Ma) and ca. 1.9 Ma, respectively. Some ages in the spectrum are centred at ca. 420, 260–300 Ma and ca. 2.5 Ga. The zircon ages from the Middle to Late Triassic samples display similar age spectra to that of the Early Triassic samples, characterized by major age peaks at 270–275 and 432 Ma and minor peaks/clusters at 790–795, 1860–1870 Ma and ca. 2.5 Ga.

Northeastern domain (i.e., NE-SG in Figure 6e)

The detrital zircon ages from the Middle and Late Triassic samples display clusters at 1.8–1.9 Ga and ca. 2.5 Ga. They noticeably lack Neoproterozic zircon populations. Middle Triassic strata yield a wider Phanerozoic age range from 270 to 510 Ma from the Late Triassic strata that are characterized by concentrated ages at 250–270 Ma and ca. 442 Ma.

Southeastern domain (i.e., SE-SG in Figure 6f)

The Middle and Late Triassic samples display similar zircon age spectra characterized by age a peak at ca. 770 Ma and an age cluster at 1.8–1.9 Ga. However, the Middle Triassic samples yield a wide range of Palaeozoic zircon ages from 270 to 490 Ma while the Late Triassic samples yield more concentrated age clusters at ca. 250–265 and 440 Ma.

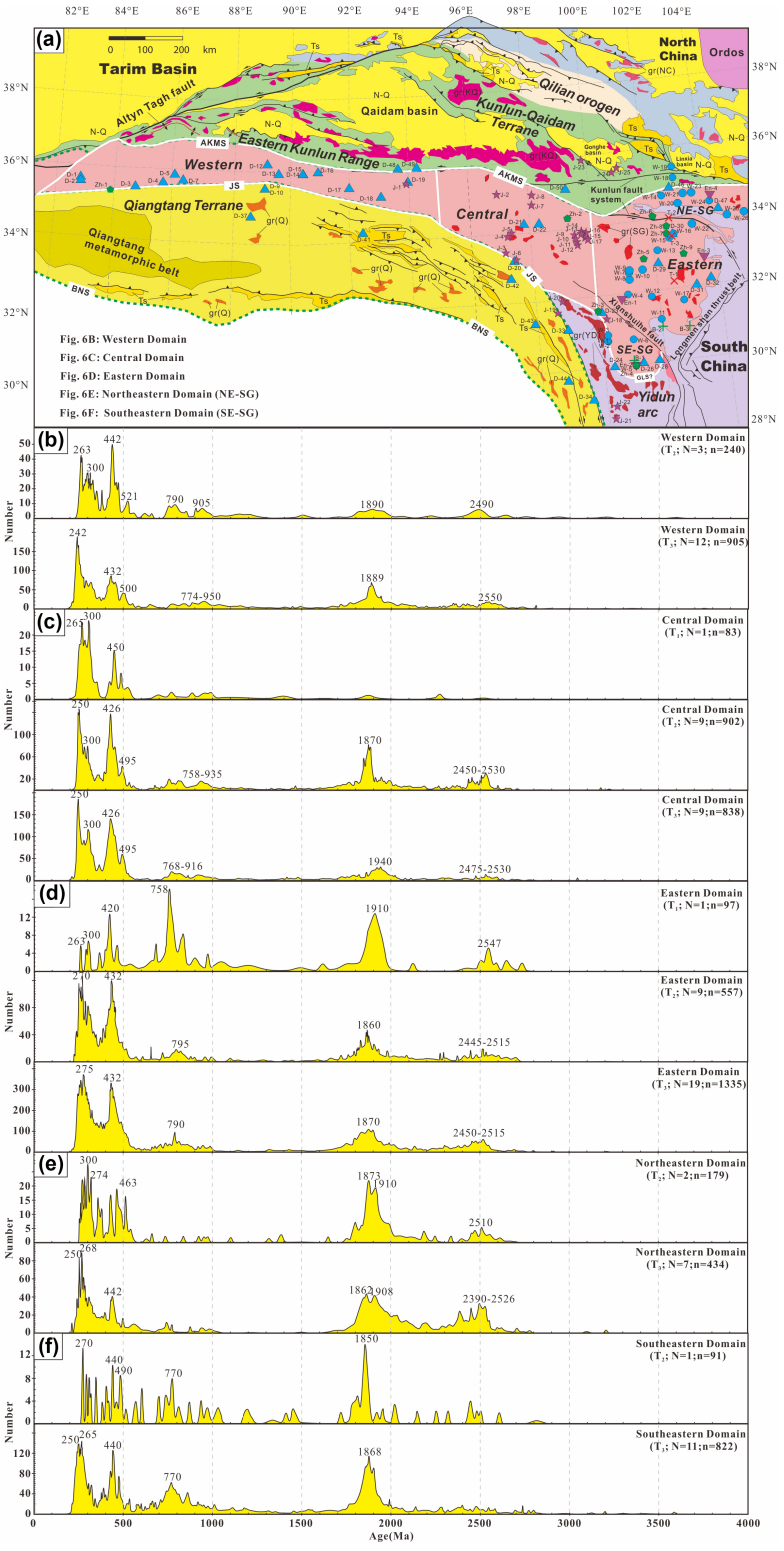

FIGURE 6 Detrital zircon U–pb ages from the Triassic strata in the Songpan-Ganzi basin. (a) Is for the spatial distributions of detrital-zircon ages, (b) is for the western domain, (c) is for the central domain, (d) is for the eastern domain, (e) is for the northeastern domain and (f) is for the southeastern domain.

5.1.2 | Kolmogorov–Smirnov tests

Using the software package available from the LaserChron Center at the University of Arizona, we performed Kolmogorov–Smirnov (K-S) tests of the Triassic samples from the Songpan-Ganzi basin. The K-S results can be found in the Table S7 that contains the '*p*' value for each compared sample pair. The *p*-value must exceed .05 to be 95% confident that the two populations are not statistically different.

Figure 7 shows that the *p*-values between samples from the northeastern domain (NE-SG) and other samples are much <.05, indicating that the compared samples are not from the same population. The *p*-value between the Middle and Late Triassic samples from the southeastern domains is 0.206, which requires the two stratigraphic sequences to have shared similar source areas. The *p*-value of = .405 indicates that the detrital zircon was derived from a similar source for samples from the southeastern and eastern domain. The western, central and eastern domains show a great similarity in source areas, which is indicated by the $p = .221$, $p = .207$, and $p = .313$ among the Middle and Late Triassic samples. Based on the K-S tests, we conclude that the Middle and Late Triassic strata in the western, central and eastern domains share similar source areas, while the northeastern and southeastern differ significantly in their source areas from those for the three domains.

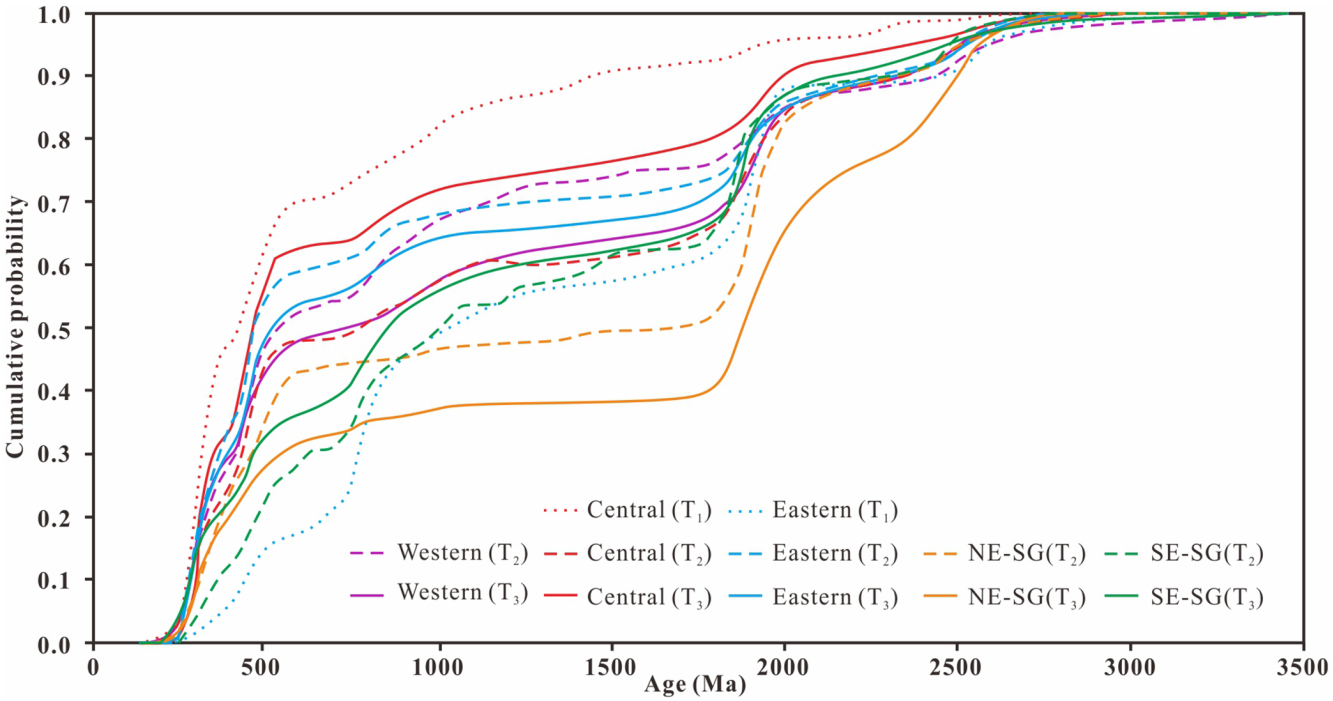

K-S test *P* value	Western (T_2)	Western (T_3)	Central (T_1)	Central (T_2)	Central (T_3)	Eastern (T_1)	Eastern (T_2)	Eastern (T_3)	NE-SG (T_2)	NE-SG (T_3)	SE-SG (T_2)	SE-SG (T_3)
Western (T_2)		0.021	0.007	0.004	0.018	0.000	0.313	0.207	0.000	0.000	0.000	0.000
Western (T_3)	0.021		0.000	0.221	0.000	0.000	0.000	0.000	0.000	0.000	0.002	0.000
Central (T_1)	0.007	0.000		0.000	0.051	0.000	0.006	0.000	0.000	0.000	0.000	0.000
Central (T_2)	0.004	0.221	0.000		0.000	0.000	0.000	0.002	0.001	0.000	0.001	0.000
Central (T_3)	0.018	0.000	0.051	0.000		0.000	0.099	0.000	0.000	0.000	0.000	0.000
Eastern (T_1)	0.000	0.000	0.000	0.000	0.000		0.000	0.000	0.001	0.000	0.405	0.003
Eastern (T_2)	0.313	0.000	0.006	0.000	0.099	0.000		0.125	0.000	0.000	0.000	0.000
Eastern (T_3)	0.207	0.000	0.000	0.002	0.000	0.000	0.125		0.000	0.000	0.000	0.000
NE-SG (T_2)	0.000	0.000	0.000	0.001	0.000	0.001	0.000	0.000		0.002	0.014	0.001
NE-SG (T_3)	0.000	0.000	0.000	0.000	0.000	0.000	0.000	0.000	0.002		0.000	0.000
SE-SG (T_2)	0.000	0.002	0.000	0.001	0.000	0.405	0.000	0.000	0.000	0.000		0.206
SE-SG (T_3)	0.000	0.000	0.000	0.000	0.000	0.003	0.000	0.000	0.000	0.000	0.206	

FIGURE 7 Cumulative distribution plots (top) and K-S test results (bottom) of detrital zircon age from the Triassic samples in the Songpan-Ganzi basin. Note that *p*-value must exceed .05 to be 95% confident that the two populations are not statistically different.

TABLE 1 Model results showing source contributions (%) based on cross-correlation coefficient

Detrital zircon										Igneous zircon				Comparison methods		
Mixed samples (domain/age)	Source-1	Source-2	Source-3	Source-4	Source-5	Source-6	Source-7	Source-8	Source-9	Source-10	Source-11	Source-12	Source-13	R^2	V	D
Western/T_2	5.37	4.20	3.35	4.79	5.16	10.38	4.71	6.79	2.41	38.31	0.79	13.07	0.66	0.300	0.245	0.142
	5.32	1.75	1.99	1.63	2.30	74.30	8.77	2.77	1.17					0.170	0.373	0.289
Western/T_3	10.51	2.66	1.88	4.40	4.00	4.62	5.94	4.28	2.79	4.58	0.67	52.98	0.67	0.520	0.184	0.119
	36.39	4.44	2.61	2.68	3.27	31.22	13.26	4.18	1.95					0.110	0.341	0.292
Central/T_1	2.50	3.39	3.38	3.11	4.28	4.50	12.06	4.67	2.56	11.26	0.88	46.68	0.73	0.160	0.377	0.208
	1.27	2.87	1.50	1.23	1.65	10.72	76.66	2.74	1.36					0.03	0.48	0.478
Central/T_2	16.08	4.39	3.81	4.38	3.92	7.74	6.89	4.52	3.57	10.58	0.91	32.59	0.63	0.45	0.202	0.129
	25.98	4.68	3.30	2.73	2.89	46.26	8.26	3.44	2.45					0.20	0.35	0.26
Central/T_3	5.09	4.50	2.83	3.86	3.83	6.57	8.78	3.54	3.03	15.53	0.82	41.14	0.49	0.52	0.217	0.135
	3.92	2.60	2.17	1.06	1.90	76.96	7.87	2.44	1.07					0.15	0.44	0.381
Eastern/T_1	32.59	5.48	15.54	5.05	9.96	5.96	3.35	9.89	5.26	2.95	0.97	2.45	0.56	0.49	0.158	0.093
	35.05	4.52	24.08	3.94	7.07	9.22	5.36	6.33	4.43					0.55	0.148	0.099
Eastern/T_2	9.99	3.08	4.09	4.74	5.46	12.32	8.40	8.38	5.10	12.62	1.00	13.76	0.73	0.380	0.247	0.152
	7.16	2.08	1.75	1.65	1.98	76.36	5.24	2.58	1.21					0.120	0.436	0.356
Eastern/T_3	10.32	3.59	3.09	4.06	4.45	10.08	6.74	5.11	3.51	16.09	0.92	31.50	0.54	0.350	0.23	0.142
	13.16	2.26	1.58	1.57	2.62	62.76	11.93	2.24	1.88					0.130	0.388	0.307
NE-SG/T_2	65.06	2.56	1.70	1.98	3.14	4.47	7.08	3.16	2.02	5.10	0.97	2.07	0.70	0.340	0.244	0.155
	61.85	2.91	2.00	1.93	2.92	10.63	12.34	3.60	1.83					0.340	0.324	0.254
NE-SG/T_3	68.70	2.18	2.40	2.79	2.73	2.55	2.47	3.08	1.94	3.20	0.89	6.25	0.83	0.360	0.223	0.142
	78.72	2.50	2.01	1.79	2.44	3.78	3.69	4.06	1.02					0.330	0.353	0.223
SE-SG/T_2	26.03	7.37	9.67	6.80	7.68	4.64	13.82	7.35	3.04	10.04	0.90	2.05	0.62	0.190	0.163	0.096
	27.43	7.06	9.60	3.74	7.09	5.99	26.79	9.55	2.76					0.210	0.181	0.131
SE-SG/T_3	27.51	5.00	5.97	5.90	6.97	5.50	4.56	7.02	4.61	3.09	1.22	21.74	0.90	0.500	0.145	0.094
	37.94	4.01	8.87	3.14	4.75	23.07	7.45	5.82	4.94					0.250	0.248	0.219

Note: Source-1 = North China Block; Source-2 = North Qinling terrane; Source-3 = South Qinling terrane; Source-4 = South China Block; Source-5 = the westernmost South China (i.e., the Longmen Shan region); Source-6 = the southern margin of the Kunlun-Qaidam terrane (i.e., the Eastern Kunlun Range); Source-7 = the northern margin of the Kunlun-Qaidam terrane (i.e., the combined North Qaidam and the Qilian orogen); Source-8 = Qiangtang terrane; Source-9 = Yidun basement; Source-10 = igneous rocks from North Qinling; Source-11 = igneous rocks from South Qinling; Source-12 = igneous rocks from the Eastern Kunlun Range; Source-13 = igneous rocks from the Yidun Arc; R^2 values for the cross-correlation coefficient; V values for the Kuiper test; D values for the Kolmogorov–Smirnov test.

TABLE 2 Model results showing source contributions (%) based on K-S test *D* value

Detrital zircon										Igneous zircon				Comparison methods		
Mixed samples (domain/age)	Source-1	Source-2	Source-3	Source-4	Source-5	Source-6	Source-7	Source-8	Source-9	Source-10	Source-11	Source-12	Source-13	R^2	*V*	*D*
Western/T_2	5.51	7.55	4.05	5.33	5.80	11.86	5.76	7.91	5.08	19.10	3.24	16.11	2.70	0.300	0.245	0.142
	2.50	2.91	2.32	1.98	1.87	81.48	2.55	2.38	2.01					0.170	0.373	0.289
Western/T_3	15.59	5.09	3.87	10.25	6.98	6.30	5.43	5.92	4.68	4.80	3.89	23.04	4.16	0.520	0.184	0.119
	1.77	2.87	2.58	1.81	1.60	74.70	2.36	10.21	2.09					0.110	0.341	0.292
Central/T_1	3.04	5.17	5.06	3.97	5.14	8.37	6.26	5.82	4.67	5.30	4.12	40.51	2.56	0.160	0.377	0.208
	1.87	3.43	2.16	1.61	2.23	81.03	2.42	3.56	1.69					0.03	0.48	0.478
Central/T_2	17.34	6.44	4.26	9.29	5.24	6.20	5.04	5.23	4.35	11.23	3.69	19.16	2.54	0.45	0.202	0.129
	2.18	2.06	2.13	1.94	2.07	82.68	2.76	2.37	1.81					0.20	0.35	0.26
Central/T_3	4.80	6.28	4.13	4.09	5.37	7.73	7.55	4.64	4.85	11.56	1.99	35.44	1.58	0.52	0.217	0.135
	1.60	2.71	2.56	1.63	2.25	82.88	2.01	2.64	1.71					0.15	0.44	0.381
Eastern/T_1	19.58	9.71	7.69	7.63	8.30	8.48	7.65	11.89	7.91	4.05	2.53	2.59	1.99	0.49	0.158	0.093
	17.92	7.71	14.32	4.93	8.20	21.42	8.13	14.02	3.35					0.55	0.148	0.099
Eastern/T_2	7.39	7.09	6.57	7.59	6.12	8.43	6.02	8.47	5.26	10.13	3.71	8.88	2.79	0.380	0.247	0.152
	2.25	2.15	2.10	2.31	2.15	81.09	3.35	2.81	1.79					0.120	0.436	0.356
Eastern/T_3	11.91	5.76	6.31	7.37	4.88	6.81	6.67	6.22	4.72	11.06	4.14	20.55	3.60	0.350	0.23	0.142
	2.37	2.54	2.04	1.91	2.37	80.89	3.33	2.40	2.14					0.130	0.388	0.307
NE-SG/T_2	32.89	4.88	4.15	5.44	5.08	6.27	5.82	5.08	3.71	8.56	4.85	9.03	4.23	0.340	0.244	0.155
	16.95	5.28	4.66	5.47	4.24	35.88	18.39	5.60	3.53					0.340	0.324	0.254
NE-SG/T_3	46.62	3.21	3.48	5.69	4.69	3.71	3.81	4.45	3.35	4.48	4.83	6.72	4.96	0.360	0.223	0.142
	33.94	7.10	4.87	4.84	4.42	29.13	5.76	6.49	3.44					0.330	0.353	0.223
SE-SG/T_2	17.89	8.22	5.77	6.73	7.75	10.96	10.50	11.23	4.06	7.72	2.79	4.27	2.13	0.190	0.163	0.096
	14.23	6.73	5.78	4.68	6.19	42.02	9.50	7.85	3.02					0.210	0.181	0.131
SE-SG/T_3	18.44	6.83	5.24	9.48	6.28	7.46	6.94	6.27	4.88	5.92	3.78	14.64	3.82	0.500	0.145	0.094
	3.54	4.76	2.70	3.65	3.82	55.40	4.38	18.67	3.08					0.250	0.248	0.219

Note: Source-1 = North China Block; Source-2 = North Qinling terrane; Source-3 = South Qinling terrane; Source-4 = South China Block; Source-5 = the westernmost South China (i.e., the Longmen Shan region); Source-6 = the southern margin of the Kunlun-Qaidam terrane (i.e., the Eastern Kunlun Range); Source-7 = the northern margin of the Kunlun-Qaidam terrane (i.e., the combined North Qaidam and Qilian orogen); Source-8 = Qiangtang terrane; Source-9 = Yidun basement; Source-10 = igneous rocks from North Qinling; Source-11 = igneous rocks from South Qinling; Source-12 = igneous rocks from the Eastern Kunlun Range; Source-13 = igneous rocks from the Yidun Arc; R^2 values for the cross-correlation coefficient; *V* values for the Kuiper test; *D* values for the Kolmogorov–Smirnov test.

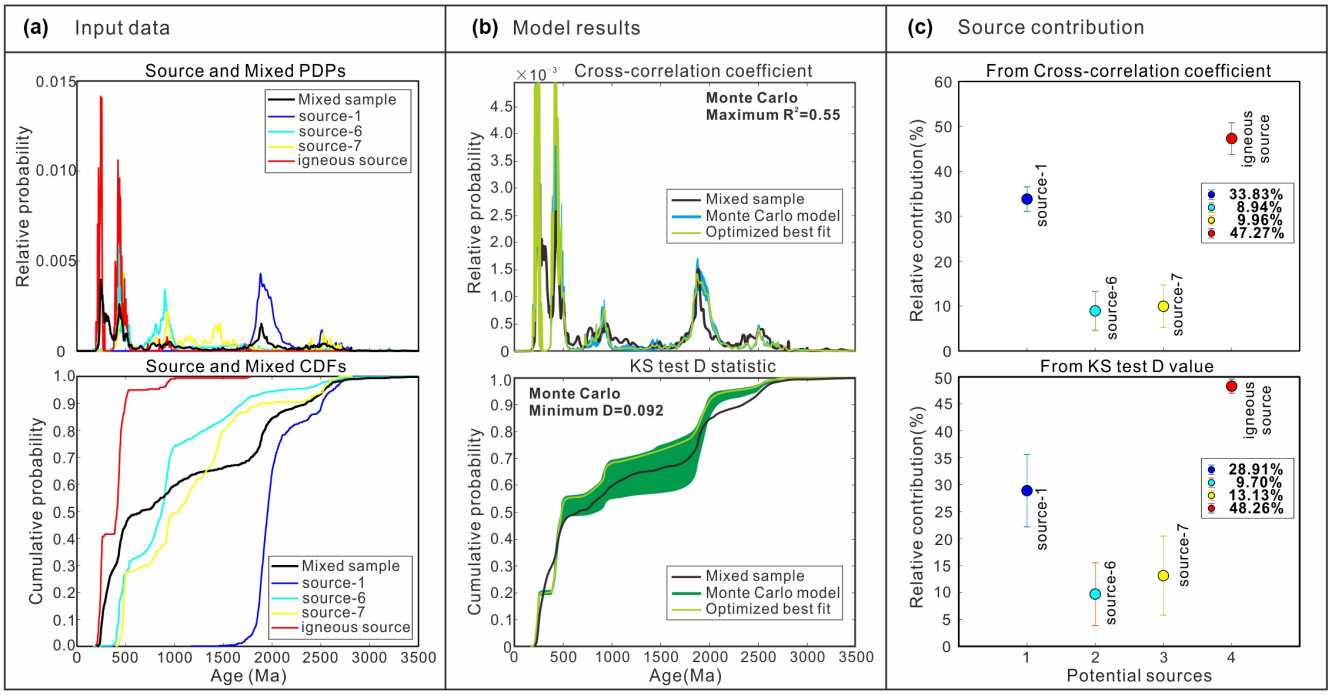

FIGURE 8 Data and model results of Triassic samples from the western domain. (a) Input mixed sample data of Triassic sandstones from the western domain and source sample data from the potential sources (Source-1 = North China block; Source-6 = the southern margin of the Kunlun-Qaidam terrane (i.e., the Eastern Kunlun range); Source-7 = the northern margin of the Kunlun-Qaidam terrane (i.e., the combined North Qaidam and Qilian orogen); igneous source = the Eastern Kunlun and/or North Qinling igneous rocks) shown as probability density plots (PDPs, top) and cumulative distribution functions (CDFs, bottom). (b) Model results using cross-correlation coefficient as probability density plots (blue, top) and the KS test D statistic as cumulative distribution functions (green, bottom). (c) Plots of the relative contribution of the potential sources by cross-correlation coefficient (top) and the KS test *D* value (bottom).

5.1.3 | DZmix analysis

Model results are shown in the Table S8. Tables 1 and 2 present the results of the relative contribution in percentage from each potential source for the analysed Triassic samples based on cross-correlation coefficient R^2 and KS test D values, respectively. Although DZmix is designed for detrital geochronology data, the source contribution of potential igneous rocks cannot be ignored. The model results (Tables 1 and 2) show that adding igneous sources increase the cross-correlation R^2 value and decrease the KS D values for all but one Triassic samples. This result means that adding the igneous source does a better job of matching the Triassic sample age distributions. However, all the model results yield an imperfect match for the Triassic samples with a maximum $R^2 = 0.55$ and a minimum D value of 0.093. The poor model fits may result from small sample size. Ideally, the sample size should be >100 (Sundell & Saylor, 2017). In our case, the sample size is 83 for the Early Triassic age data from the central domain, 97 for the Early Triassic age data from the eastern domain, 91 for the Middle Triassic age data from the southeastern domain, 88 for the North Qinling age data, 56 for the South Qinling age data and 41 for the Yidun age data. Another cause of poor model fits may come from source age populations that do not contribute to the mixed sample age distribution. Finally, the igneous zircon age data with the data size labelled as N have different geological meanings from the size of detrital zircon age data labelled as n. That is, a small sample size of an igneous age population may make un-proportionally larger contributions to the mixing models obtained using the DZmix approach. The above discussion indicates that uncertainties in the DZmix model results can be mitigated by increasing the sample size and extracting those with greater relative contribution as potential source samples. Below, we summarize the main features of the DZmix modelling results.

Western domain modelling results (Figure 8a–c)

The best matching model is generated by increasing sample size and by exacting realistic source samples from North China, the southern margin (i.e., the Eastern Kunlun Range) and northern margin (i.e., the combined North Qaidam and the Qilian orogen) of the Kunlun-Qaidam terrane, and igneous sources from the Eastern Kunlun Range and North Qinling orogen. Figure 8b shows

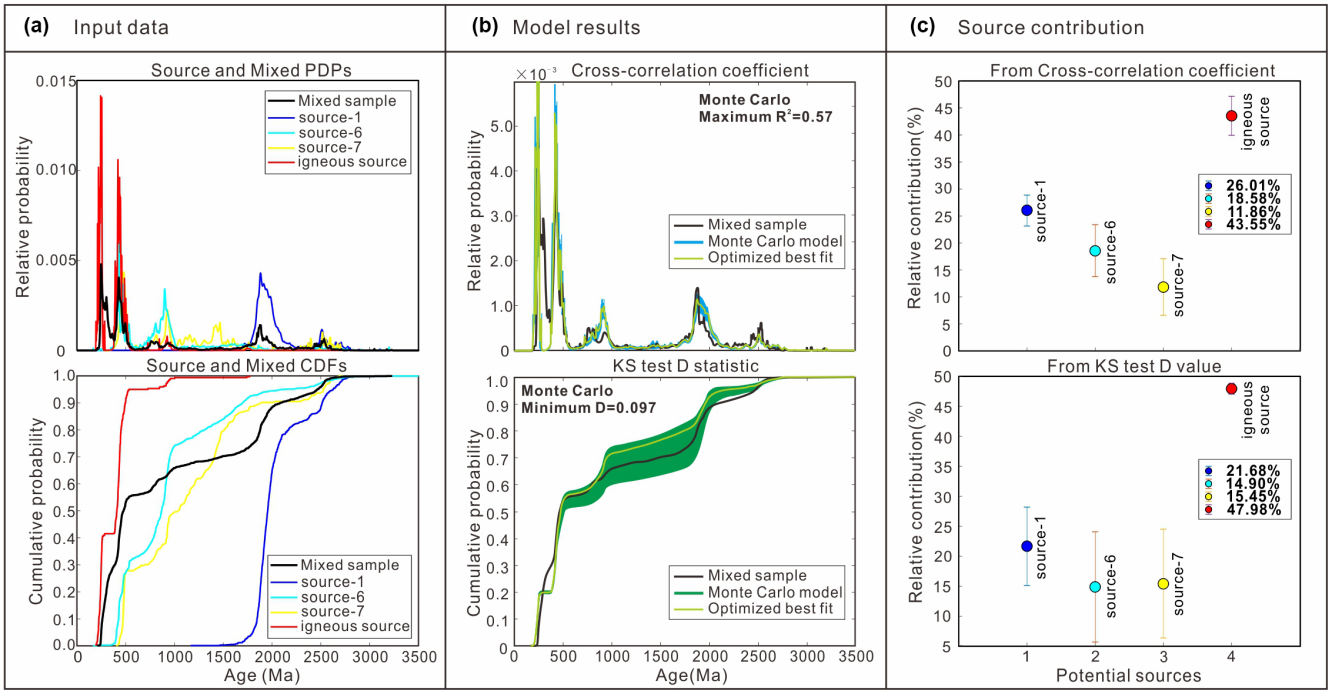

FIGURE 9 Data and model results of Triassic samples from the central domain. (a) Input mixed sample data of Triassic sandstones from the central domain and source sample data from the potential sources (Source-1 = North China block; Source-6 = the southern margin of the Kunlun-Qaidam terrane (i.e., the Eastern Kunlun Range); Source-7 = the northern margin of the Kunlun-Qaidam terrane (i.e., the combined North Qaidam and Qilian orogen); igneous source = the Eastern Kunlun and/or North Qinling igneous rocks) shown as probability density plots (PDPs, top) and cumulative distribution functions (CDFs, bottom). (b) Model results using cross-correlation coefficient as probability density plots (blue, top) and the KS test *D* statistic as cumulative distribution functions (green, bottom). (c) Plots of the relative contribution of the potential sources by cross-correlation coefficient (top) and the KS test *D* value (bottom).

the best fit model results that require $R^2 = 0.55$, minimum $D = 0.092$, a mean of 0.55 ± 0.001 and a standard deviation of 0.097 ± 0.003. But no model yields a perfect fit due to a poor match of the mixed sample age distribution between 0–500 and 2000–2500 Ma. This disharmony may be explained by the difference in abundance between the igneous and detrital zircon age data, and by the overestimation of NCB sources, respectively. Figure 8c shows the relative contribution of potential sources from cross-correlation coefficient R^2 and KS test *D* value, respectively. The plot shows that the Middle and Late Triassic samples from the wesern domain were mainly sourced from the Eastern Kunlun area and/or North Qinling orogenic belt (47.27%–48.26%), the NCB (28.91%–33.83%), the Eastern Kunlun basement (8.94%–9.70%) and the combined North Qaidam and the Qilian orogen (9.96%–13.13%).

Central domain modelling results (Figure 9a–c)

The model result is similar to that for the western domain data. Considering that only one Early Triassic sample (sample D-22 with $n = 83$; see Figure 1 for sample location) is reported by Ding et al. (2013) with the *p*-value (Figure 7) between Early (T_1) and Late Triassic (T_3) samples to exceed .05, modelling is carried out between mixed age data from Early to Late Triassic samples and potential source age data from North China, the Eastern Kunlun basement, the combined northern Kunlun-Qaidam terrane and the early Palaeozoic Qilian orogen, and igneous zircon ages from the Eastern Kunlun and/or the North Qinling orogen. Figure 9b shows the model results for $R^2 = 0.57$, minimum $D = 0.097$, a mean of 0.57 ± 0.001, and a standard deviation of 0.101 ± 0.002. Misfit is most prominent for the central domain age data between 0 and 500 Ma and/or between 2000 and 2500 Ma due to the unavoidable igneous sources. Figure 9c shows the relative contribution of potential sources from the Eastern Kunlun and/or North Qinling igneous rocks (43.55%–47.98%), NCB (21.68%–26.01%), the Eastern Kunlun basement (14.90%–18.58%), and the combined North Qaidam and the Qilian orogen (11.86%–15.45%). The model results are also consistent with paleocurrent data from the area presented below.

Eastern domain modelling results (Figure 10a–c) and (Figure 11a–c)

The model result is more complex than that derived from the western and central domain age data. Although only one Early Triassic sample is used in the analysis (sample D-32 with $n = 97$; see Figure 1 for sample

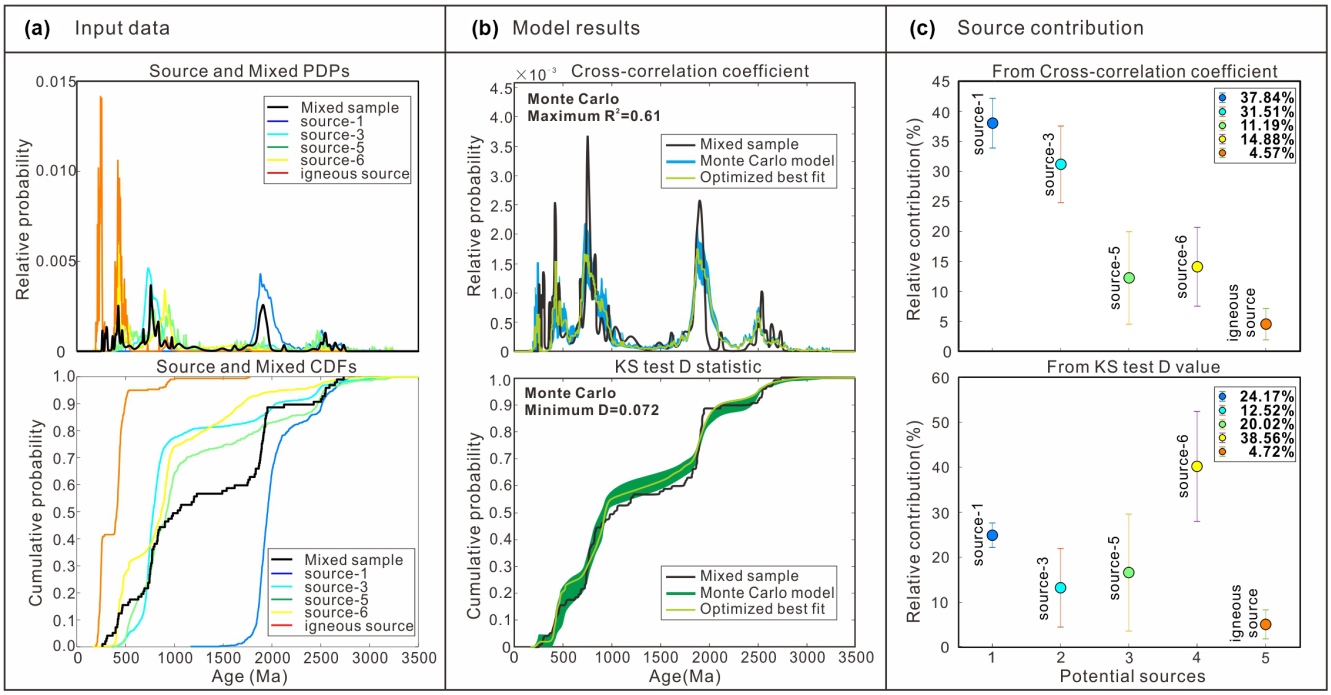

FIGURE 10 Data and model results of early Triassic samples from the eastern domain. (a) Input mixed sample data of early Triassic sandstones from the eastern domain and source sample data from the potential sources (Source-1 = North China block; Source-3 = South Qinling terrane; Source-5 = the westernmost South China (i.e., the Longmen Shan region); Source-6 = Eastern Kunlun Range basement; igneous sources = the Eastern Kunlun and/or North Qinling igneous rocks) shown as probability density plots (PDPs, top) and cumulative distribution functions (CDFs, bottom). (b) Model results using cross-correlation coefficient as probability density plots (blue, top) and the KS test *D* statistic as cumulative distribution functions (green, bottom). (c) Plots of the relative contribution of the potential sources by cross-correlation coefficient (top) and the KS test *D* value (bottom).

location), the age distribution of the Early Triassic sample differs from those of the Middle and Late Triassic samples from the eastern domain (Figure 6). In contrast, the age distribution of the Early Triassic sample is highly similar to those of the Triassic samples from the southeastern domain indicated by the *p*-value of .405 (Figure 7). Hence, the results for the eastern domain data are divided into the Early Triassic (Figure 10a–c) and Middle-Late Triassic (Figure 11a–c) models, respectively. The Early Triassic model (Figure 10b) requires $R^2 = 0.61$, minimum $D = 0.072$, a mean of 0.60 ± 0.006 and a standard deviation of 0.086 ± 0.004. Figure 10c shows the relative contribution of potential sources derived from the NCB (24.17%–37.84%), the South Qinling terrane (12.52%–31.51%), the Eastern Kunlun basement (14.88%–38.56%), the westernmost SCB in the Longmen Shan area (11.19%–20.02%) and igneous sources (4.57%–4.72%). The provenance of the Early Triassic samples (Figure 10c) from the easternmost eastern domain differs from that of Middle and Late Triassic samples (Figure 11c) from the eastern domain by a lack of igneous sources and the addition of the South Qinling basement and/or westernmost SCB (Longmen Shan) sources. The lack of igneous sources for the Early Triassic data from the eastern domain may indicate that the closure of the Paleo-Tethys oceans by suturing along the Kunlun-Qinling orogen had not started at this time. The model result is consistent with an east-derived source area as indicated by the paleocurrent data (see below) and the heavy mineral assemblage analysis of the Triassic samples located in the easternmost eastern domain (see discussion below).

Northeastern domain modelling results (Figure 12a–c)

Figure 12b shows the best-fit model result that yields $R^2 = 0.48$, minimum $D = 0.091$, a mean of 0.48 ± 0.002 and a standard deviation of 0.101 ± 0.004. Figure 12c shows the relative contribution of potential sources by the best-fit model: the NCB (56.02%–68.18%), the Eastern Kunlun and/or North Qinling igneous rocks (17.63%–31.10%), the Eastern Kunlun basement (5.05%–6.29%), and the combined North Qaidam and the Qilian orogen (7.83%–7.89%). Compared with the western, central and eastern domains, the provenance of the Triassic samples from the northeastern domain is characterized by much more contributions from a NE-derived source (e.g., NCB), less contributions from NW-derived sources (e.g., the Kunlun-Qaidam terrane and the Qilian orogen) and a significant decline in contributions from the igneous sources (i.e., igneous rocks from Eastern Kunlun and/or North Qinling).

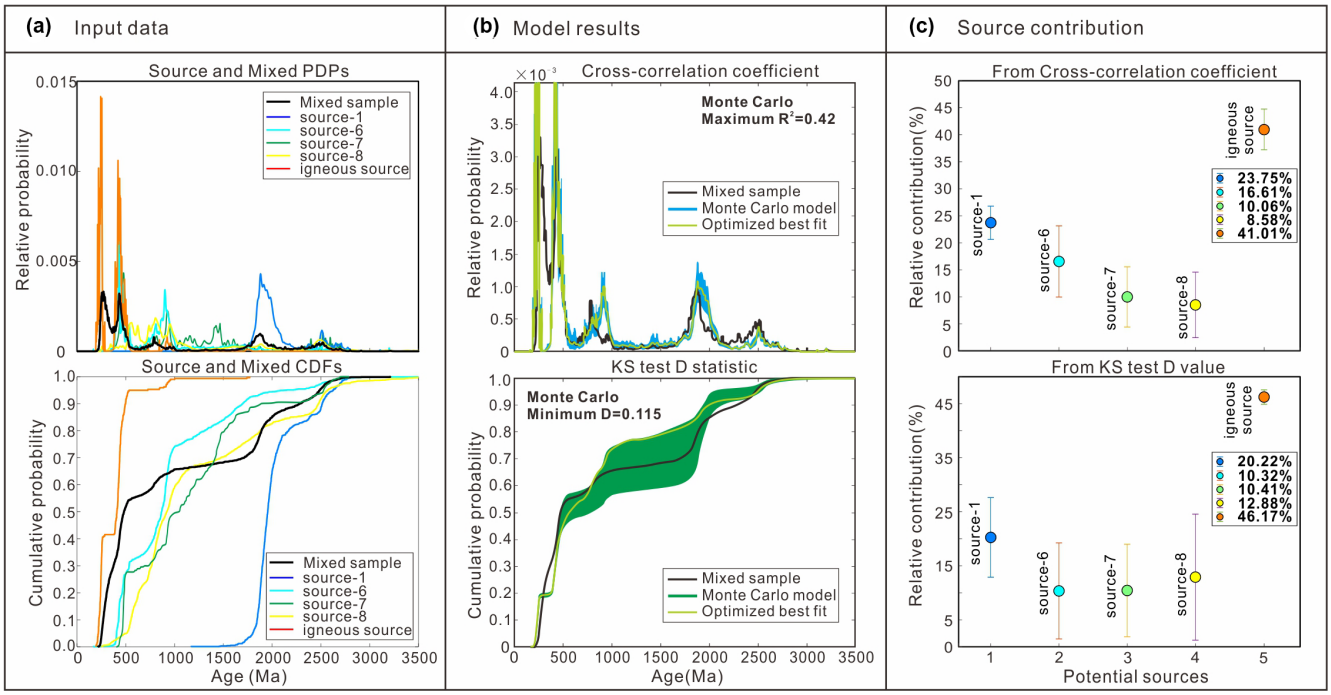

FIGURE 11 Data and model results of middle-late Triassic samples from the eastern domain. (a) Input mixed sample data of middle-late Triassic sandstones from the eastern domain and source sample data from the potential sources (Source-1 = North China block; Source-6 = the southern margin of the Kunlun-Qaidam terrane (i.e., the Eastern Kunlun Range); Source-7 = the northern margin of the Kunlun-Qaidam terrane (i.e., the combined North Qaidam and Qilian orogen); Source-8 = Qiangtang terrane; igneous sources = the Eastern Kunlun and/or North Qinling igneous rocks) shown as probability density plots (PDPs, top) and cumulative distribution functions (CDFs, bottom). (b) Model results using cross-correlation coefficient as probability density plots (blue, top) and the KS test *D* statistic as cumulative distribution functions (green, bottom). (c) Plots of the relative contribution of the potential sources by cross-correlation coefficient (top) and the KS test *D* value (bottom).

Southeastern domain modelling results (Figure 13a–c)

Figure 13b shows the best-fit model result that yields a mean of 0.57 ± 0.003 and a deviation of 0.075 ± 0.006 with a maximum R^2 value of 0.58 and a minimum *D* value of 0.059. Figure 13c shows the relative contribution of potential sources required by the best-fit models: the NCB (23.74%–32.91%), the Eastern Kunlun and/or North Qinling igneous rocks (27.32%–34.84%), the Qiangtang terrane (22.32%–28.36%) and the South Qinling basement (13.06%–17.45%). The partitioning of the source contribution differs from that for the western, central and eastern domains by an addition of the Qiangtang terrane source and a lack of contribution from the Kunlun-Qaidam terrane and the Qilian orogen.

5.2 | Paleocurrent directions during the formation of the Songpan-Ganzi basin

Figure 14 shows the paleocurrent data of Weislogel et al. (2010), Ding et al. (2013) and Jian et al. (2019) from the Triassic Songpan-Ganzi strata basin, and the result shows that (1) the western domain records mostly southward and southeastward flows, (2) the central domain records mostly southeastward and southwestward flow, (3) the eastern domain record southwestward flow and bidirectional southeastward and northwestward flows, (4) the northeastern domain records mostly southward, southeastward and southwestward flows, and (5) the southeastern domain records westward, northwestward, and southwestward flows. The above paleocurrent data indicates that the western and central domains are mainly sourced from a northern provenance that includes the Kunlun-Qinling orogen, the Kunlun-Qaidam terrane and possibly North China. The diverse paleocurrent directions from the eastern domain require both a northern provenance similar to that for the western and central domains and an additional eastern provenance in South China. The paleocurrent orientation from the northeastern domain indicates its source areas mainly from the Qinling orogen and North China in north. This contrasts to the southeastern domain whose paleocurrent data require source areas from the northwest and southwest located in South China. Note that no eastward or westward paleocurrent directions have ever been observed across the Songpan-Ganzi basin (Figure 14), which is

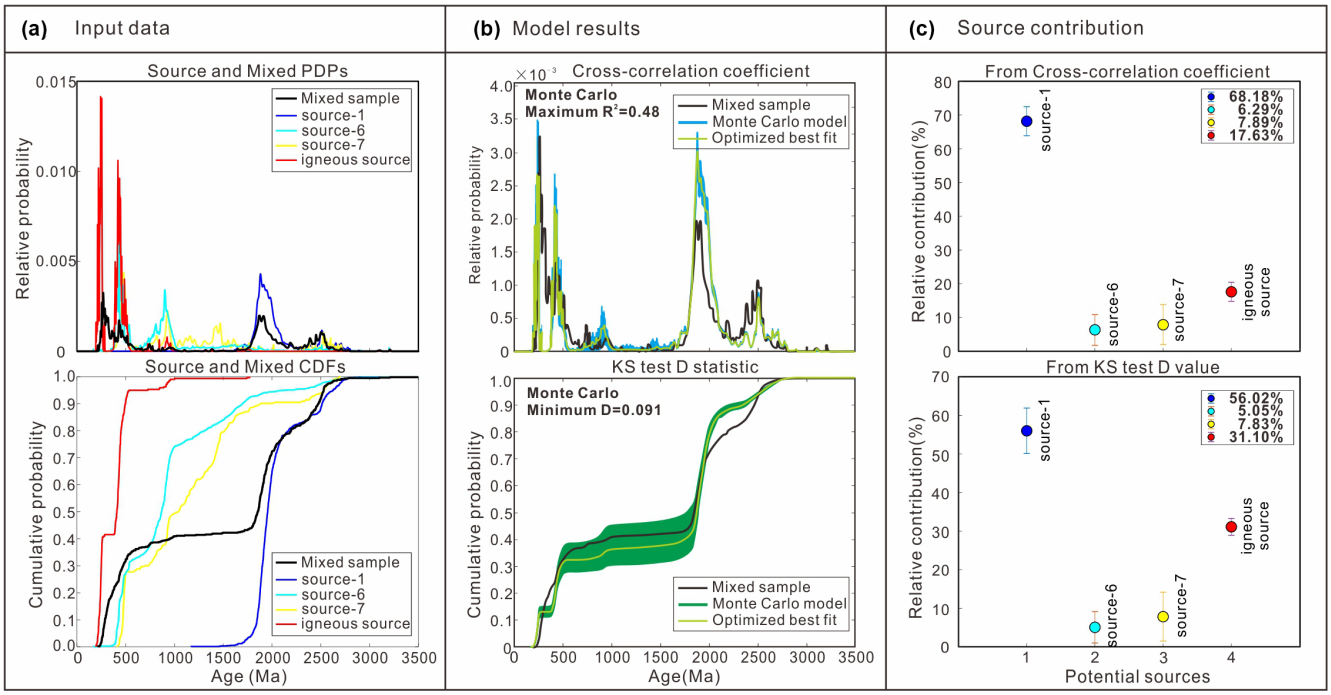

FIGURE 12 Data and model results of Triassic samples from the northeastern domain. (a) Input mixed sample data of Triassic sandstones from the northeastern domain and source sample data from the potential sources (Source-1 = North China block; Source-6 = the southern margin of the Kunlun-Qaidam terrane (i.e., the Eastern Kunlun Range); Source-7 = the northern margin of the Kunlun-Qaidam terrane (i.e., the combined North Qaidam and Qilian orogen); igneous sources = the Eastern Kunlun and/or North Qinling igneous rocks) shown as probability density plots (PDPs, top) and cumulative distribution functions (CDFs, bottom). (b) Model results using cross-correlation coefficient as probability density plots (blue, top) and the KS test *D* statistic as cumulative distribution functions (green, bottom). (c) Plots of the relative contribution of the potential sources by cross-correlation coefficient (top) and the KS test *D* value (bottom).

inconsistent with a back-arc extension-basin model that requires a large-scale (>1500 km) horizontal sediment transport systems as proposed by Ding et al. (2013).

5.3 | Sandstone petrography

Figure 15 shows the sandstones are dominated by quartz with varying amounts of feldspar and lithic fragments that are poorly rounded and poorly sorted with low compositional and textural maturity reflecting a turbidity current depositional origin in a proximal slope-basin environment with rapid erosion and burial. The result of plotting the area-count data on the ternary QmFLt diagram (Figure 15), where Qm represents monocrystalline quartz, F represents combined plagioclase and potassium feldspar, and Lt represents the total lithic fragments. The total lithic fragments in turn can be further divided into volcanic rock fragment (Lv), sedimentary rock fragment (Ls), and metamorphic rock fragment (Lm), and stable polycrystalline quartzite fragments. All samples analysed in this study are plotted in a recycled orogen or arc fields, which is consistent with the formation of the Songpan-Ganzi basin during the closure of the Paleo-Tethys ocean via subduction and development of continental arcs along the basin margins.

5.4 | Heavy mineral analysis

5.4.1 | Distribution of heavy minerals

Table 3 presents the abundances of the heavy minerals of Triassic samples from the eastern Songpan-Ganzi basin. We identify 13 heavy minerals that include zircon, apatite, rutile, tourmaline, garnet, sphene, epidote, magnetite, Fe-Ti minerals (anatase, ilmenite and leucoxene; leucoxene often regarded as alteration of ilmenite or other titanium minerals), and Fe-S minerals (haematite-limonite, pyrite and pyrrhotite). Figure 16 shows representative CL images of different zircon morphologies: (1) the 'idiomorphic' group characterized by euhedral, subhedral, elongated and zoned grains, which are mainly distributed in the Zoige County site and (2) the 'rounded' group that consists of rounded and subrounded grains, which are widely developed in the Songpan County site.

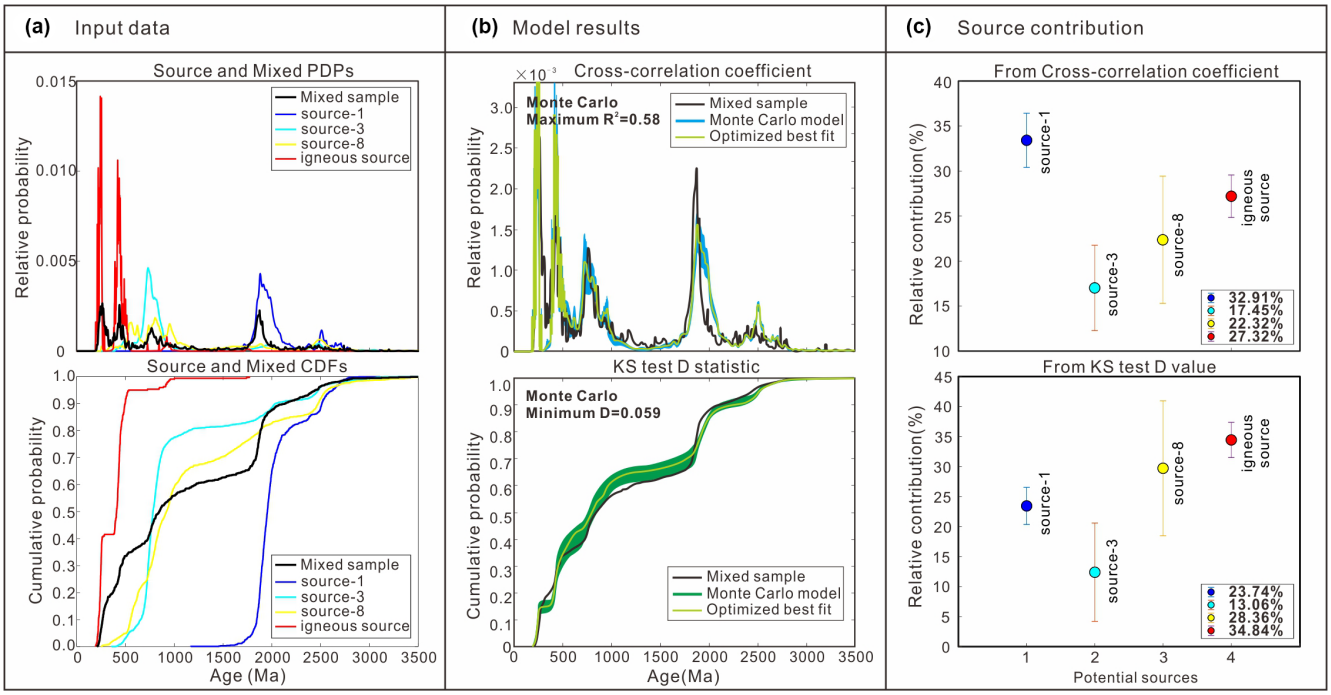

FIGURE 13 Data and model results of Triassic samples from the southeastern domain. (a) Input mixed sample data of Triassic sandstones from the southeastern domain and source sample data from the potential sources (Source-1 = North China block; Source-3 = South Qinling terrane; Source-8 = Qiangtang terrane; igneous sources = the Eastern Kunlun and/or North Qinling igneous rocks) shown as probability density plots (PDPs, top) and cumulative distribution functions (CDFs, bottom). (b) Model results using cross-correlation coefficient as probability density plots (blue, top) and the KS test *D* statistic as cumulative distribution functions (green, bottom). (c) Plots of the relative contribution of the potential sources by cross-correlation coefficient (top) and the KS test *D* value (bottom).

5.4.2 | Heavy mineral parameters

Table 3 also presents the calculation results of heavy mineral parameters including the zircon-tourmaline-rutile (ZTR) index (Hubert, 1962), the rutile-zircon (RZi) index, and the garnet-zircon (GZi) index (Morton & Hurst, 1995). The ZTR index can be used as a measure of the maturity of heavy mineral assemblages. In general, a higher ZTR index indicates more stable minerals in the hosting sediments that may imply a more distal source. ZTR values of the Triassic sandstone samples from the eastern domain vary from 2 to 60 (Table 3), which implies either mixing of detritus from proximal and distant sources of similar lithology or the same source area with highly variable lithologies (Hubert, 1962). Figure 17a shows ZTR index values in different locations from west (sites in the Zoige County) to east (sites in the Songpan County) in the study area. The lower ZTR values of less than 20 are mainly concentrated in the Songpan site, indicating a different provenance from the Zoige site samples. In addition, provenance-sensitive parameters such as the rutile/zircon ratio (RZi) and the garnet/zircon ratio (GZi) are useful to assess input of materials derived from source areas exposing high-grade metamorphic rocks. That is, high RZi and GZi indexes indicate high-grade metamorphic rocks in source areas, while low RZi and GZi indexes without rutile and garnet imply lower-grade metamorphic rocks in source areas. Significant variation in RZi and GZi values occurs throughout the study area (Figure 17b,c). The RZi values of most samples from the Zoige County site are >10. This contrasts the RZi values for all but one samples from the Songpan site that are <10. The GZi values in the Zoige County site vary from 0 to 88, and samples with higher GZi (>60) values are commonly accompanied with lower ZTR index values (i.e., samples FT-2, FT-8, FT-14, FT-17, ZL-3, and ZL-8). This correlation indicates a proximal source exposing high-grade metamorphic rocks. Meanwhile, we find that GZi values are consistently zero for samples collected from the Songpan County site. This implies the absence of garnet characteristic of high-grade metamorphic rocks in the source area. The above heavy-mineral analysis suggests that the provenance of the eastern domain of the Songpan-Ganzi basin varies from site to site.

5.4.3 | Heavy mineral assemblage and their protolith

Heavy minerals from the eastern Songpan-Ganzi basin samples can be divided into assemblages: (1) an assemblage

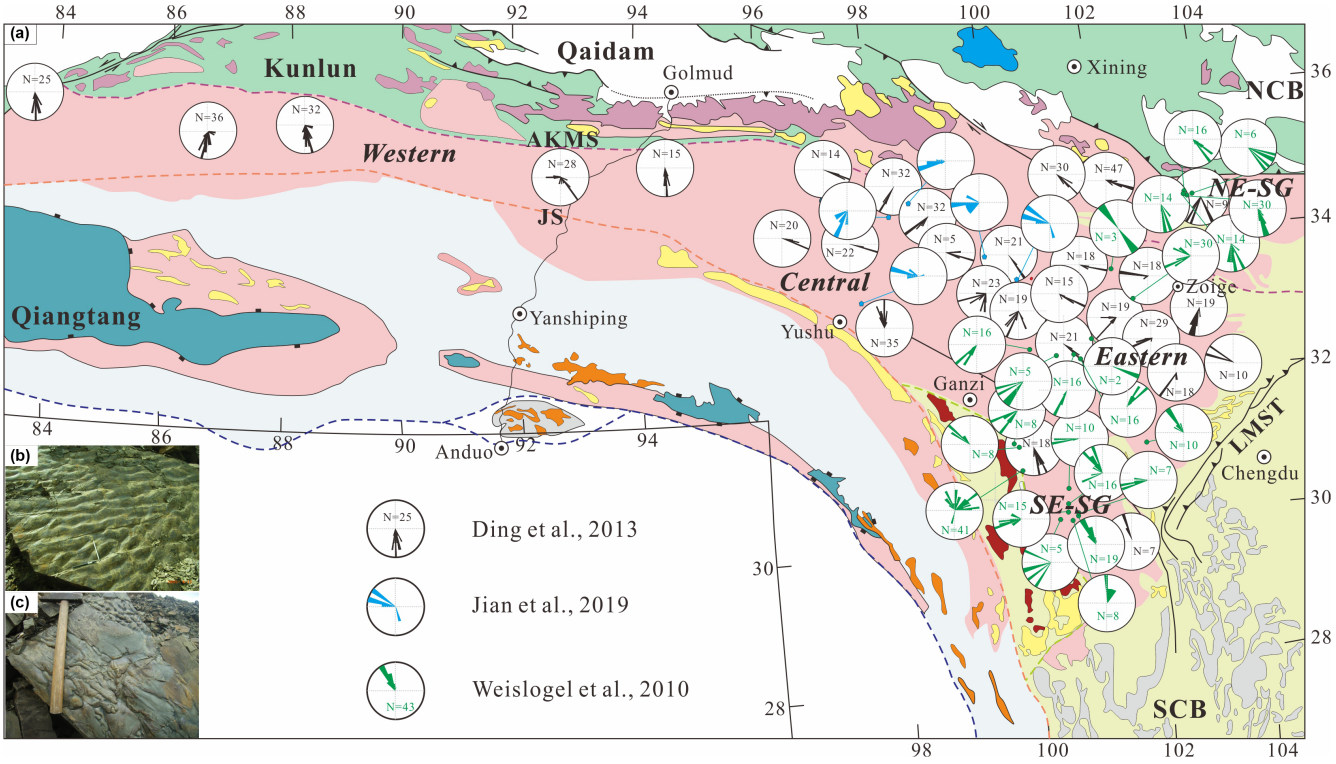

FIGURE 14 Rose diagrams of paleocurrent orientations from Triassic strata in the Songpan-Ganzi basin. (a) Rose diagrams shown inside black circles are from Ding et al. (2013); blue circles are from Jian et al. (2019); green circles are from Weislogel et al. (2010). (b,c) Ripple and flute casts observed in the Zoige County from the eastern Songpan-Ganzi basin.

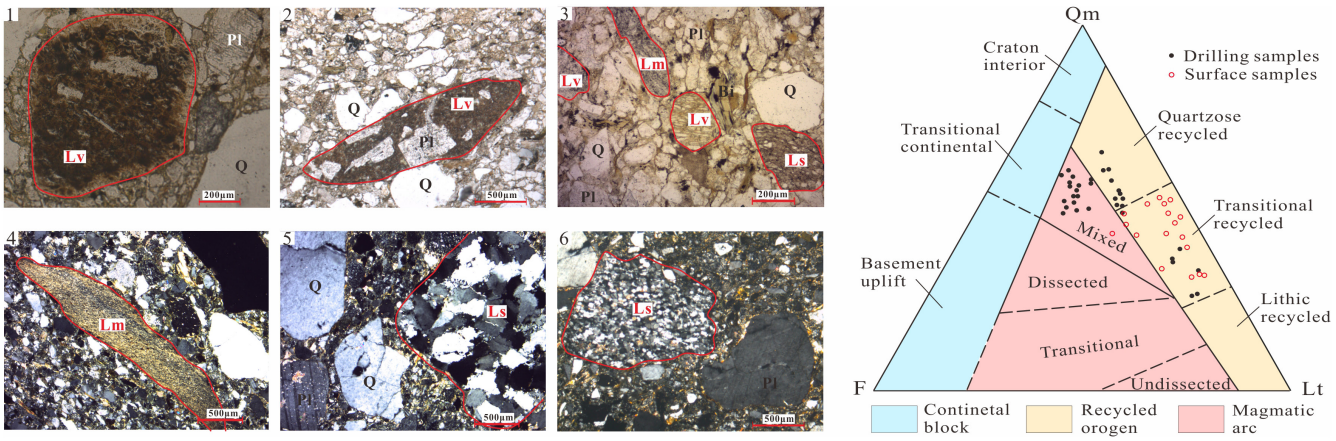

FIGURE 15 Representative microphotographs of Triassic sandstones from the eastern Songpan-Ganzi basin and the QmFLt diagram after Dickinson (1988) indicating possible provenance affiliation. Photos of 1–6 are various lithic fragments including volcanic rock fragment (lv), sedimentary rock fragment (ls), and metamorphic rock fragment (Lm). Q = quartz; pl = plagioclase; Bi = biotite; Qm = monocrystalline quartz; F = feldspar; Lt = Total lithic fragments.

consisting of apatite, sphene, zircon (colourless: euhedral, subhedral), tourmaline (brown, individually blue: idiomorphic), rutile (low RZi values) are considered to indicate acid igneous sources, (2) an assemblage consisting of Fe-Ti minerals (anatase, ilmenite, leucoxene), magnetite, Cr-spinel and pyroxene represent basic igneous and ultrabasic (commonly arc-related) sources, (3) an assemblage consisting of garnet, epidote, rutile (high RZi values) are interpreted to indicate metamorphic sources, and (4) an assemblage consisting of Fe-S minerals (pyrite, pyrrhotite, haematite-limonite), and recyclable mineral phases such as zircon, tourmaline, and rutile (with high ZTR index, e.g., quartz sandstone). Although pyrite and haematite are most likely to have an authigenic origin

TABLE 3 The abundances of the heavy minerals of the Triassic samples from the eastern Songpan-Ganzi basin (wt. %)

													Fe-Ti minerals			Fe-S minerals			Heavy mineral parameters		
SN	Location	Fm	Zr	Ap	Rt	Tur	Grt	Spn	Ep	Mag	Px	Cr-Spl	Ant	Ilm	Leu	Hem-Lm	Py	Po	ZTR	RZi	GZi
FT-1	Zoige	T_3z	28.05	13.07	10.3	6.17	4.2	4.87	2.58	0	0	0	3.16	3.37	12.37	7.46	4.39	0	44.52	26.86	13.02
FT-2	Zoige	T_3z	17.68	5.07	2.89	5.77	32.92	15.92	0	0	0	0	0.42	2.49	4.97	11.86	0	0	26.34	14.05	65.06
FT-3	Zoige	T_3z	32.84	21.74	3.48	4.86	7.37	11.94	0	3.1	0	0	0	0.46	1.26	11.14	1.8	0	41.18	9.58	18.33
FT-5	Zoige	T_2zg	20.72	19.88	2.15	5.88	2.93	5.19	0	0	0.45	0	0	2.32	21.77	16.56	2.15	0	28.75	9.40	12.39
FT-6	Zoige	T_3z	47.21	11.47	7.75	4.34	0.93	0	0.72	0	0.31	0	9.81	8.06	5.37	2.89	1.14	0	59.30	14.10	1.93
FT-7	Zoige	T_2zg	21.96	26.22	2.8	6.01	0	2.33	0	0	0	0	1.09	2.24	11.46	25.89	0	0	30.77	11.31	0.00
FT-8	Zoige	T_3zh	1.63	1.12	0.4	2.4	12.25	0	9.35	17.28	1.16	0	0.07	46.18	0.09	7.94	0.14	0	4.43	19.70	88.26
FT-9	Zoige	T_3zh	43.64	24.45	5.64	7.05	0.72	3.01	0	1.2	0	0	0	0	12.3	0.19	1.81	0	56.33	11.44	1.62
FT-10	Zoige	T_3zh	36.87	5.53	9.05	3.44	13.76	4.75	0	0	1.15	0	5.94	9.55	4.47	4.22	1.27	0	49.36	19.71	27.18
FT-11	Zoige	T_3x	38.93	20.02	5.7	4.14	2.5	13.42	0	0	0	0	0	2.42	7.23	5.63	0	0	48.77	12.77	6.03
FT-12	Zoige	T_3z	20.21	16.53	4.15	11.38	20.01	11.61	0	1.47	0	0	0.57	1.36	2.09	10.63	0	0	35.74	17.04	49.75
FT-13	Zoige	T_3z	21.45	13.93	4.74	5.85	1.3	0	6.5	0	1.11	0	2.04	11.23	26	5.85	0	0	32.04	18.10	5.71
FT-14	Zoige	T_3zh	4.45	4.02	1.88	1.43	35.74	2.87	0	14.06	0	0	0	0	0.7	34.85	0	0	7.76	29.70	88.93
FT-15	Hongyuan	T_3z	19.42	3.98	1.98	12.43	9.05	0	18.13	0	1.78	0	1.17	5.38	0	26.23	0.46	0	33.83	9.25	31.79
FT-16	Hongyuan	T_2zg	36.16	19.71	3.77	1	1.69	5.21	0	5.9	0	0	1.63	1.57	13.37	8.91	1.07	0	40.93	9.44	4.46
FT-17	Hongyuan	T_2zg	17.45	9.77	1.22	13.74	33.71	0	7.18	4.52	0	0	2.5	2.44	2.9	3.86	0.72	0	32.41	6.53	65.89
FT-18	Hongyuan	T_3zh	33.56	17.67	4.25	3.31	1.74	5.91	0	0	0	0	0	0	7.34	14.45	11.77	0	41.12	11.24	4.93
FT-19	Hongyuan	T_2zg	21.28	4.49	3.24	6.94	4.43	0.86	1.26	0	0.93	0	1.32	2.51	7.53	41.97	3.24	0	31.46	13.21	17.23
HY-2	Hongyuan	T_2zg	28.68	26.21	3.32	5.33	9.17	0	0	0	0	0.09	0.42	0	23.87	2.9	0	0	37.33	10.38	24.23
HY-4	Hongyuan	T_2zg	19.37	10.57	3.04	4.05	0	0	0	0	0	0	0.16	0	42.57	20.25	0	0	26.46	13.57	0.00
HY-7	Hongyuan	T_2zg	28.26	22.82	4.35	10.66	6.42	0	0	0	0	0.41	0	0	26.39	0.68	0	0	43.27	13.34	18.51
HY-8	Hongyuan	T_3z	23.81	14.19	3.47	8.27	17.23	0	0	0	0	0.7	0.16	0	31.82	0.35	0	0	35.55	12.72	41.98
HY-9	Hongyuan	T_3z	27.97	21.72	3.75	3.37	8.06	0	0	0	0	0.36	0.16	0	33.23	0.24	1.15	0	35.09	11.82	22.37
ZL-1	Zhangla	T_2zg	24.81	4.4	3.16	2.08	37.25	0	0	0	0	0.64	0.45	0	23.38	3.84	0	0	30.05	11.30	60.02
ZL-3	Zhangla	T_2zg	20.6	12.84	3.34	2.87	39.25	0	0	0	0	0.68	0.53	0	19.2	0.55	0.14	0	26.81	13.95	65.58
ZL-5	Zhangla	T_2zg	7.87	5.14	1.45	1.8	0.22	0	0	0	0	0.22	0.16	0	9.66	38	35.48	0	11.12	15.56	2.72
ZL-6	Zhangla	T_3z	17.87	27.3	2.16	2.5	0	0	0	0	0	0.25	0.2	0	25.73	23.78	0.2	0	22.53	10.78	0.00
ZL-7	Zhangla	T_3z	33.45	12.72	1.96	5.59	2.02	0	0	0	0	1.19	0.59	0	41.64	0.83	0	0	41.00	5.54	5.69
ZL-8	Zhangla	T_2zg	5.73	7.42	0.6	0.77	25.9	0	0	0	0	0	0.22	0	3.29	56.09	0	0	7.10	9.48	81.88
ZL-10-3	Zhangla	T_3z	28.03	11.4	1.74	5.32	25.19	0	0	0	0	1.77	0.63	0	21.29	4.61	0	0	35.09	5.84	47.33
SP-SS-2	Songpan	T_3zh	3.68	10.18	0	9.47	0	0	0	0	0	0	0.04	72.5	0	4.13	0	0	13.15	0.00	0.00
SP-4	Songpan	T_3x	11.24	4.26	1.54	4.45	0	0	0	0	0	0	0	0	0	0	78.52	0	17.23	12.05	0.00

TABLE 3 (Continued)

SN	Location	Fm	Zr	Ap	Rt	Tur	Grt	Spn	Ep	Mag	Px	Cr-Spl	Fe-Ti minerals			Fe-S minerals			Heavy mineral parameters		
													Ant	Ilm	Leu	Hem-Lm	Py	Po	ZTR	RZi	GZi
SP-7	Songpan	T_3x	27.41	2.44	3.25	4.68	0	0	0	0	0	0	0	0	1.02	56.85	4.36	0	35.34	10.60	0.00
SP-9	Songpan	T_3z	2.24	3.44	0	0.63	0	0	0	0	0	0	0	85.97	0	0.21	0	7.51	2.87	0.00	0.00
SP-10	Songpan	T_3zh	5.38	24.38	0.18	22.5	0	0	0	0	0	0	0	0	0	47.56	0	0	28.06	3.24	0.00
SP-11	Songpan	T_3x	27.64	2.94	0.44	6.34	0	0	0	0	0	0	13.52	0	0	44.7	4.41	0	34.42	1.57	0.00
SP-12	Songpan	T_3z	7.05	12.4	0.64	0.44	0	0	0	0	0	0	0	0	3.85	64.94	10.69	0	8.13	8.32	0.00
SP-15	Songpan	T_3zh	29.15	0.72	1.45	9.33	0	0	0	0	0	0	0.15	0	7.69	41.93	9.57	0	39.93	4.74	0.00
SP-16	Songpan	T_3zh	45.83	6.85	2.88	11.02	0	0	0	0	0	0	2.4	0	11.04	14.21	5.76	0	59.73	5.91	0.00
SP-19	Songpan	T_3x	5.81	0.2	0.45	4.53	0	0	0	0	0	0	0.08	0	1.39	83.03	4.5	0	10.79	7.19	0.00
SP-21	Songpan	T_3x	1.4	0.81	0.07	0.24	0	0	0	0	0	0	0	0	0	37.18	60.29	0	1.71	4.76	0.00
SP-23	Songpan	T_3x	18.01	1.77	0.3	0.13	0	0	0	0	0	0	0	0	0.3	34.87	44.64	0	18.44	1.64	0.00
SP-25	Songpan	T_3zh	5.79	12.48	0	0	0	0	0	0	0	0	0	0	0	54.59	27.14	0	5.79	0.00	0.00
SP-27	Songpan	T_3zh	44.59	0.86	9.69	5.46	0.1	0	0	0	0	0	0.61	1.43	0	29.99	3.93	3.35	0	59.74	17.85	0.22

Note: SN = Sample Number; Fm. = Formation; Zr = Zircon; Ap = Apatite; Rt = Rutile; Tur = Tourmaline; Grt = Garnet; Spn = Sphene; Ep = Epidote; Mag = Magnetite; Px = Pyroxene; Cr-Spl = Cr-Spinel; Ant = Anatase; Ilm = Ilmenite; Leu = Leucoxene; Hem-Lm = Haematite-limonite; Py = Pyrite; Po = Pyrrhotite.

with an intrabasinal source, the large fraction of such minerals in the analysed samples (i.e., from 50% to 90%) requires an explanation. Based on field observations, we find that Silurian carbonaceous phyllite in the Longmen Shan area of the easternmost Songpan-Ganzi basin contains abundant pyrite and haematite (Figure 18c). This observation led to suggest that the Longman Shan area of westernmost South China was the primary source area of the large amount of pyrite and haematite in our analysed heavy-mineral samples.

Figure 18 shows the source-rock types required by the heavy mineral assemblages obtained from this study. Heavy minerals in samples collected from sites in the Zoige County require mainly felsic to mafic igneous rocks with a minor contribution from metamorphic and sedimentary rocks in the source areas (Figure 18a). The most likely source area is the Kunlun-Qinling orogen where intruded by large Phanerozoic plutonic rocks (Figure 5a,b). This interpretation implies a northerly derived source area consistent with the paleocurrent data (Figure 14). Heavy minerals in samples collected from sites in the Songpan County require the source-area rock types to be mainly sedimentary, followed by minor contributions from felsic to mafic igneous rocks (Figure 18b). The most likely source area that meets this requirement is the Longmen Shan area of western South China where a thick section of Neoproterozoic to Jurassic strata area exposed (Pan et al., 2004). This interpretation is consistent with the paleocurrent data from this area (Figure 14).

6 | DISCUSSION

Table 4 summarizes the interpreted source areas of the Songpan-Ganzi basin constrained by combined quantitative DZmix modelling, paleocurrent data, sandstone petrography and heavy mineral analysis. Our DZmix modelling shows that the northern Songpan-Ganzi basin had a stable northern source system that includes North China, the combined Kunlun-Qaidam terrane and the Qilian orogen, and the Kunlun-Qinling orogen. The eastern basin also had a stable source system that consists of the South Qinling terrane and westernmost South China in the Longmen Shan area. Similarly, the southeastern basin was sourced from two stable source systems: the Qiangtang terrane in the west and southwest and western South China in the east and northeast.

Sandstones petrography from the eastern part of the Songpan-Ganzi basin shows that the Triassic sediments were deposited in a recycled orogen and/or in a mixed magmatic arc. The required tectonic setting is consistent with the Songpan-Ganzi basin located within the Paleo-Tethys

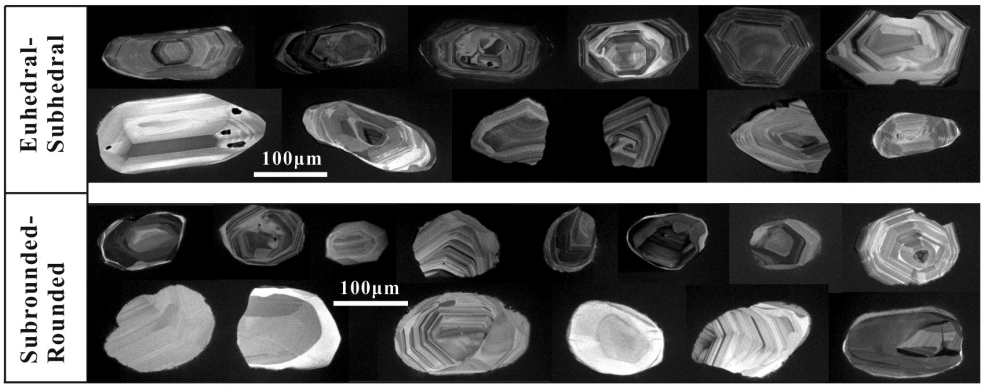

FIGURE 16 Representative CL images of different zircon morphologies.

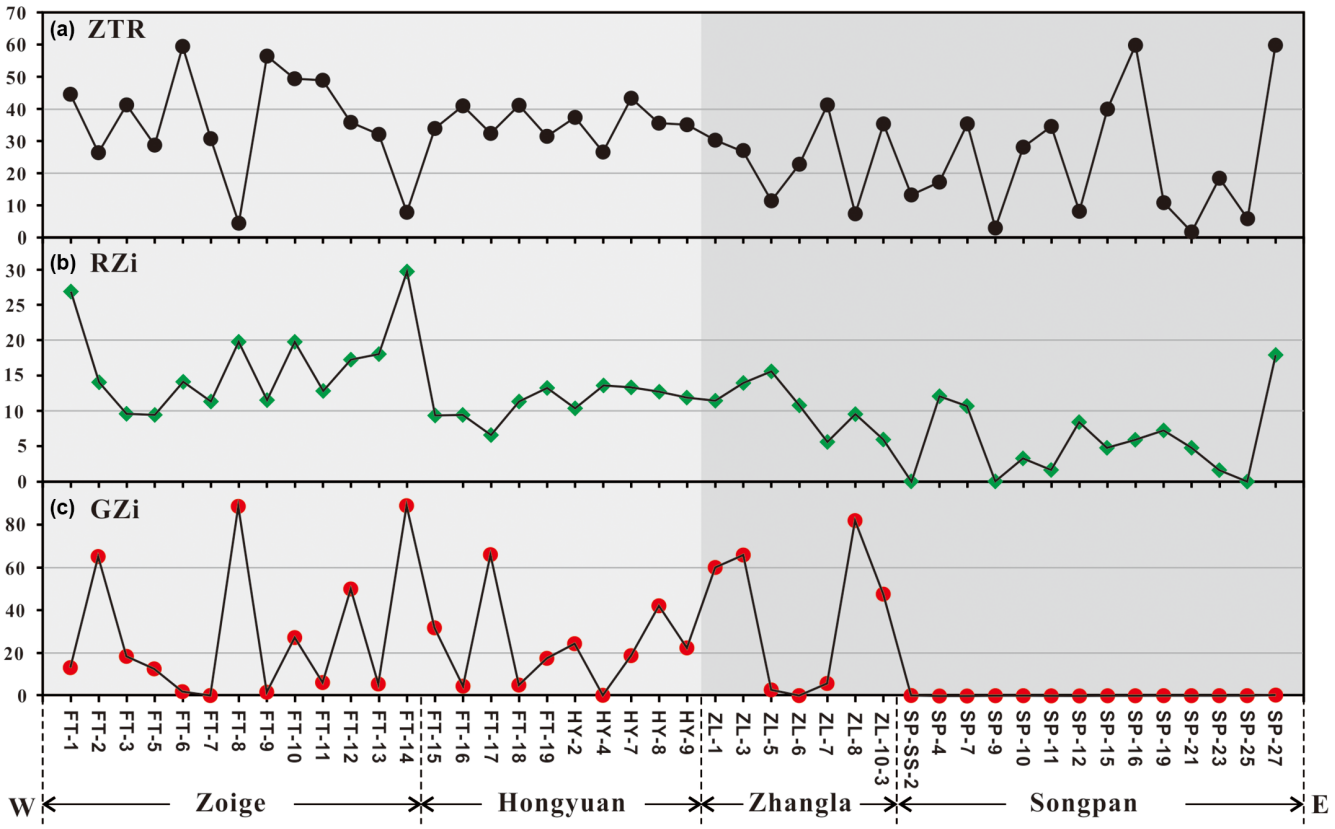

FIGURE 17 Variations in the ZTR, RZi and GZi index of the Triassic samples from the eastern Songpan-Ganzi basin. ZTR, RZi and GZi are determined as given in Table 3. ZTR = zircon + tourmaline + rutile; RZi = 100 × rutile/(rutile + zircon); GZi = 100 × garnet/(garnet + zircon). Horizontal coordinates represent the sampling sites from west (Figure 18a) to east (Figure 18b)

ocean and next to the continental arc developed along the basin-bounding Kunlun-Qaidam terrane (Wu et al., 2016; Yin & Harrison, 2000). Our heavy mineral analysis shows that the eastern part of the Songpan-Ganzi basin was mainly sourced from felsic to basic igneous rocks, which are best correlated to the Kunlun-Qinling orogen as the potential source area (Wu et al., 2016; Yin & Harrison, 2000). The sandstone composition and heavy mineral assemblages requires the easternmost part of the Songpan-Ganzi basin was mainly derived from a recycled sedimentary source best correlated to those exposed in the western South China margin exposed in the Longmen Shan area (Pan et al., 2004; Wang, Pan, et al., 2013). This interpretation is consistent with our DZmix modelling result.

The stable and locally derived detritus for the deposition of the Songpan-Ganzi basin (i.e., the northern

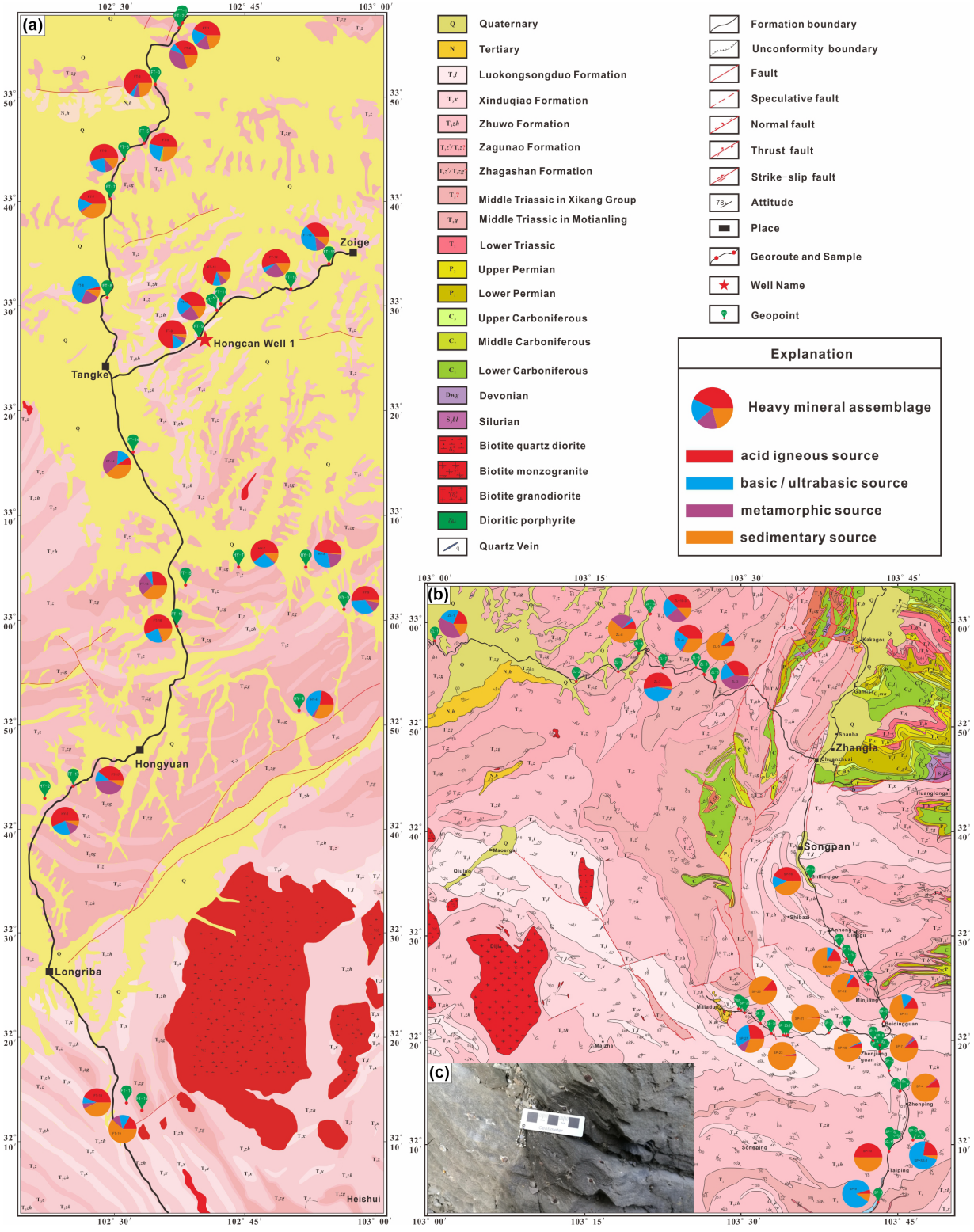

FIGURE 18 The distribution of source rocks based on heavy mineral assemblage from the eastern Songpan-Ganzi basin (the study area enlarged from Figure 1). (a) Is for sites in the Zoige County; (b) is for sites in the Songpan County; (c) is photograph of Silurian bearing pyrite carbonaceous phyllite in the Longmen Shan area of the easternmost Songpan-Ganzi basin.

basin has a northern source and the eastern basin has an eastern source) is most consistent with the remnant ocean model that predicts the basin to have been bounded by approaching continental terrains and cratonal blocks during the closure of the Paleo-Tethys ocean (Nie et al., 1994; Weislogel et al., 2006, 2010; Zhou &

TABLE 4 The provenance of the Songpan-Ganzi basin constrained by a synthesis of multi-proxy provenance data

Songpan-Ganzi basin	DZmix modelling results							Paleocurrent directions	Result of sandstone composition	Result of heavy mineral analysis
	Source-1	Source-3	Source-5	Source-6	Source-7	Source-8	Igneous sources			
Western	28.91%–33.83%	/	/	8.94%–9.70%	9.96%–13.13%	/	47.27%–48.26%	S, SE	/	/
Central	21.68%–26.01%	/	/	14.90%–18.58%	11.86%–15.45%	/	43.55%–47.98%	SE, SW	/	/
Eastern	20.22%–23.75%	/	/	10.32%–16.61%	10.06%–10.41%	8.58%–12.88%	41.01%–46.17%	SW, SE, NW	In a recycled orogen or arc field	Mainly derived from acid to basic igneous rocks
Easternmost	24.17%–37.84%	12.52%–31.51%	11.19%–20.02%	14.88%–38.56%	/	/	4.57%–4.72%	W, NW	/	Mainly sourced from pyrite-bearing sedimentary rocks
Northeastern	56.02%–68.18%	/	/	5.05%–6.29%	7.83%–7.89%	/	17.63%–31.10%	S, SE, SW	/	/
Southeastern	23.74%–32.91%	13.06%–17.45%	/	/	/	22.32%–28.36%	27.32%–34.84%	W, NW, SW	/	/

Note: Source-1 = North China Block; Source-3 = South Qinling terrane; Source-5 = the westernmost South China (i.e., the Longmen Shan region); Source-6 = the southern margin of the Kunlun-Qaidam terrane (i.e., the Eastern Kunlun Range); Source-7 = the northern margin of the Kunlun-Qaidam terrane (i.e., the combined North Qaidam and the Qilian orogen); Source-8 = Qiangtang terrane; Igneous sources = the Eastern Kunlun and/or North Qinling igneous rocks.

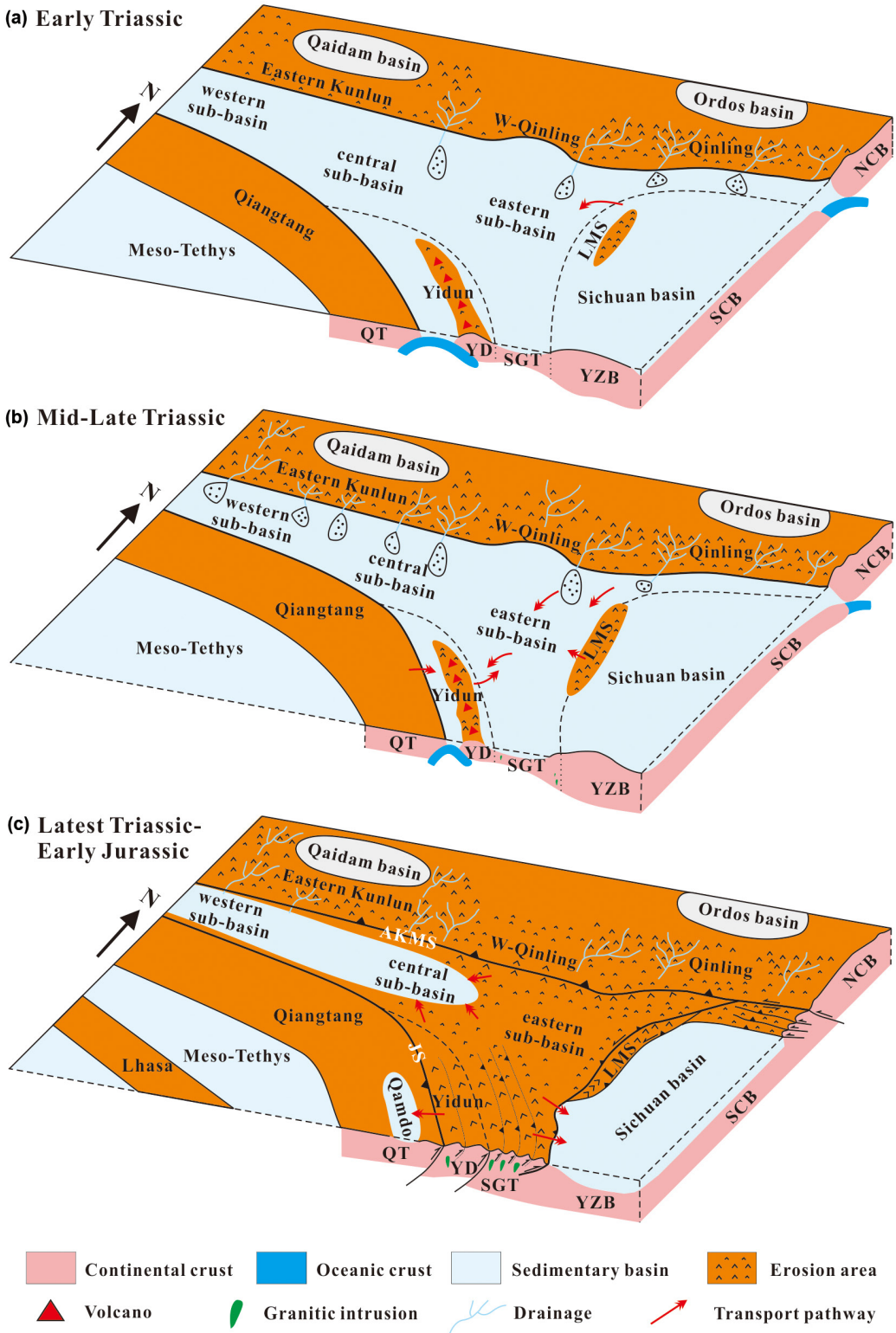

Graham, 1996). In contrast, a stable source system for the Songpan-Ganzi basin is inconsistent with the mobilistic model proposed by Pullen et al. (2008) and Ding et al. (2013), which requires migration of the Yidun arc across the Songpan-Ganzi basin as it was opened by slab rollback during the closure of the Paleo-Tethys ocean. The southward migration of the Yidun arc rifted from the southern margin of Asia in the Pullen et al. (2008) model would in turn require a progressive change in source areas from the Kunlun-Qaidam terrane to the Qiangtang terrane and western South China, which is not consistent with the results obtained in this study.

A synthesis of multi-proxy provenance data allows us to construct a coherent Triassic tectonic model for the

FIGURE 19 Sketched tectonic model for the Triassic development of the Songpan-Ganzi basin. (a) In the early Triassic, the western and central sub-basins were subducting northward during which the easternmost sub-basin received locally derived materials from the northwestern margin of South China (see Figure 10). (b) In the middle to late Triassic, the western, central and eastern sub-basins were sourced mainly from the northern bounding regions (e.g., North China, the combined Kunlun-Qaidam terrane and the Qilian orogen, and the Kunlun-Qinling orogen; see Figures 8, 9, and 11). At this time, the northeastern margin of the Songpan-Ganzi basin and Triassic strata in the western Qinling orogen have similar detrital-zircon age populations (Figures 4b and 6e), which can be interpreted as sharing the same source areas from North China and the Kunlun-Qinling orogen (Figure 12). Meanwhile, the Triassic strata in the southeastern margin of the Songpan-Ganzi basin contain similar detrital-zircon age populations to those of Triassic sediments in the Yidun arc (Figures 4f and 6f), which best correlated to the source rocks in the Qiangtang terrane and western South China (Figure 13). (c) Since the latest Triassic to the early Jurassic, the final closure of the paleo-Tethyan Ocean was accomplished by the convergence and collision among North China, South China, and the Qiangtang terrane. AKMS, Anyimaqen-Kunlun-Mianlue suture; JS, Jinsha suture; NCB, North China block; QT, Qiangtang terrane; SCB, South China block; SGT, Songpan-Ganzi terrane; YD, Yidun terrane; YZB, Yangtze block.

development of the Songpan-Ganzi basin (Figure 19). In our model, the basement of the Songpan-Ganzi basin is assumed to be a highly extended and thinned continental crust of South China (Wu et al., 2016 and references therein), and the Yidun arc was originated by rifting from South China. In the Early Triassic (Figure 19a), the western and central sub-basins were subducting northward during which the easternmost sub-basin received locally derived materials from the northwestern margin of South China (see Figure 10). In the Middle to Late Triassic (Figure 19b), the western, central and eastern sub-basins were sourced mainly from the northern bounding regions (e.g., North China, the combined Kunlun-Qaidam terrane and the Qilian orogen, and the Kunlun-Qinling orogen) (see Figures 8, 9, 11). At this time, the northeastern margin of the Songpan-Ganzi basin and Triassic strata in the western Qinling orogen have similar detrital-zircon age populations (Figures 4b and 6e), which can be interpreted as sharing the same source areas from North China and the Kunlun-Qinling orogen (Figure 12). Meanwhile, the Triassic strata in the southeastern margin of the Songpan-Ganzi basin contain similar detrital-zircon age populations to those of Triassic sediments in the Yidun arc (Figures 4f and 6f), which best correlated to the source rocks in the Qiangtang terrane and western South China (Figure 13). Between the latest Triassic and the Early Jurassic (Figure 19c), the final closure of the Paleo-Tethyan ocean was accomplished by the convergence and eventual collision among North China, South China and the Qiangtang terrane (Nie et al., 1994; Weislogel et al., 2006, 2010; Zhou & Graham, 1996). The final collision is expressed by intense folding of the Late Triassic turbidite strata in the Songpan-Ganzi basin (Burchfiel & Chen, 2012).

7 | CONCLUSIONS

In this paper, we systematically reviewed the available provenance data of the Triassic Songpan-Ganzi basin deposits from literature. The data include U–Pb detrital zircon ages at the basin scale, paleocurrent directions and sandstone petrography. Our original contribution to this study is the heavy mineral analysis of Triassic samples from the eastern part of the Songpan-Ganzi basin. Our synthesis of the multi-proxy provenance data shows that the Songpan-Ganzi basin had a stable and locally derived source system: the northern basin was mainly sourced from the north (North China, the combined Kunlun-Qaidam terrane and the Qilian orogen, and the Kunlun-Qinling orogen), the eastern basin was sourced from the east (South China), and the southeastern basin was sourced from both the west (Qiangtang) and east (South China). The stability of the source areas around the Songpan-Ganzi basin throughout the Triassic is compatible with the remnant ocean model that predicts a long-lived marine basin with a pre-Triassic oceanic/continental basement trapped between converging continental blocks during the closure of the Paleo-Tethys ocean, rather than the mobilistic model requires migration of the Yidun arc across the Songpan-Ganzi basin as it was opened by slab rollback during the closure of the Paleo-Tethys ocean. The southward migration of the Yidun arc rifted from the southern margin of Asia in the Pullen et al. (2008) model would in turn require a progressive change in source areas from the Kunlun-Qaidam terrane to the Qiangtang terrane and western South China, which is not consistent with our provenance results. The provenance results in this study are consistent with the early work of Weislogel et al. (2006, 2010) who reached a similar conclusion. Although our current data analysis does not support the slab-rollback model of Pullen et al. (2008) for the Triassic development of the Songpan-Ganzi basin, more systematic studies that integrate source rocks and basin deposits are needed in the future.

ACKNOWLEDGEMENTS

This work was supported by the National Natural Science Foundation of China (41302047, 41702044) and the Natural Science Foundation of Shaanxi Province

(2018JM4003). All data are provided in the present manuscript and Tables S1 (sample information from Triassic strata in the Songpan-Ganzi basin), S2 (zircon age data of igneous rocks from the Songpan-Ganzi basin), S3 (detrital zircon U–Pb age data from potential basement rocks), S4 (detrital zircon U–Pb age data from contemporary Triassic strata around the Songpan-Ganzi basin), S5 (zircon U–Pb ages from potential igneous rocks), S6 (detrital zircon U–Pb age data from Triassic strata in the Songpan-Ganzi basin), S7 (K-S testing result of Triassic samples from the Songpan-Ganzi basin), and S8 (results of the DZmix modelling between Triassic samples and source samples).

PEER REVIEW

The peer review history for this article is available at https://publons.com/publon/10.1111/bre.12703.

DATA AVAILABILITY STATEMENT

The data that support the findings of this study are openly available in [repository name] at [DOI].

REFERENCES

Bruguier, O., Lancelot, J. R., & Malavieille, J. (1997). U-pb dating on single detrital zircon grains from the Triassic Songpan-Ganzi flysch (Central China): Provenance and tectonic correlations. *Earth and Planetary Science Letters*, *152*, 217–231.

Burchfiel, B. C., & Chen, Z. (Eds.). (2012). *Tectonics of the southeastern Tibetan plateau and its adjacent foreland* (Vol. *210*). Geological Society of America.

Bureau of Geology and Mineral Resources of Qinghai Province (BGMRQP). (1991). *Regional geology of Qinghai Province (in Chinese)*. Geological Publishing House.

Bureau of Geology and Mineral Resources of Sichuan Province (BGMRSP). (1991). *Regional geology of Sichuan Province (in Chinese)*. Geological Publishing House.

Chang, E. Z. (2000). Geology and tectonics of the Songpan-Ganzi fold belt, southwestern China. *International Geology Review*, *42*(9), 813–831.

Chen, Q., Sun, M., Long, X. P., Zhao, G. C., & Yuan, C. (2016). U–pb ages and hf isotopic record of zircons from the late Neoproterozoic and Silurian–Devonian sedimentary rocks of the western Yangtze block: Implications for its tectonic evolution and continental affinity. *Gondwana Research*, *31*, 184–199.

Chen, W. T., Zhou, M. F., & Zhao, X. F. (2013). Late paleoproterozoic sedimentary and mafic rocks in the Hekou area, SW China: Implication for the reconstruction of the Yangtze block in Columbia. *Precambrian Research*, *231*, 61–77.

Chen, X. H., George, G., Yin, A., Li, L., & Jiang, R. B. (2012). Paleozoic and Mesozoic basement magmatisms of eastern Qaidam basin, northern Qinghai-Tibet plateau: LA-ICP-MS zircon U-pb geochronology and its geological significance. *Acta Geologica Sinica (English Edition)*, *86*(2), 350–369.

Dai, J. G., Wang, C. S., Hourigan, J., & Santosh, M. (2013). Multi-stage tectono-magmatic events of the eastern Kunlun range, northern Tibet: Insights from U–pb geochronology and (U–Th)/He thermochronology. *Tectonophysics*, *599*, 97–106.

Darby, B. J., & Gehrels, G. (2006). Detrital zircon reference for the North China block. *Journal of Asian Earth Science*, *26*(6), 637–648. https://doi.org/10.1016/j.jseaes.2004.12.005

De Sigoyer, J., Vanderhaeghe, O., Duchene, S., & Billerot, A. (2014). Generation and emplacement of Triassic granitoids within the Songpan Ganze accretionary-orogenic wedge in a context of slab retreat accommodated by tear faulting, eastern Tibetan plateau, China. *Journal of Asian Earth Sciences*, *88*, 192–216.

Dewey, J. F., Shackleton, R. M., Chang, C. F., & Sun, Y. Y. (1988). The tectonic evolution of the Tibetan plateau. *Philosophical Transactions of the Royal Society of London, A*, *327*, 379–413. https://doi.org/10.1098/rsta.1988.0135

Dickinson, W. R. (1988). Provenance and sediment dispersal in relation to paleotectonics and paleogeography of sedimentary basins. In K. Kleinspehn & C. Paola (Eds.), *New perspectives in basin analysis* (pp. 3–25). Springer Verlag.

Dickinson, W. R., Beard, L. S., Brakenridge, G. R., Erjavic, J. L., Ferguson, R. C., Inman, K. F., Knepp, R. A., Lindeberg, F. A., & Ryberg, P. T. (1983). Provenance of north American phanerozoic sandstones in relation to tectonic setting. *Geological Society of American Bulletin*, *94*, 222–235.

Ding, L., Yang, D., Cai, F. L., Pullen, A., Kapp, P., Gehrels, G. E., & Shi, R. D. (2013). Provenance analysis of the Mesozoic Hoh-Xil-Songpan-Ganzi turbidites in northern Tibet: Implications for the tectonic evolution of the eastern paleo-Tethys Ocean. *Tectonics*, *32*, 34–48.

Ding, Q. F., Jiang, S. Y., & Sun, F. Y. (2014). Zircon U–pb geochronology, geochemical and Sr–Nd–hf isotopic compositions of the Triassic granite and diorite dikes from the Wulonggou mining area in the eastern Kunlun orogen, NW China: Petrogenesis and tectonic implications. *Lithos*, *205*, 266–283.

Ding, Q. F., Liu, F., & Yan, W. (2015). Zircon U–pb geochronology and hf isotopic constraints on the petrogenesis of early Triassic granites in the Wulonggou area of the eastern Kunlun orogen, Northwest China. *International Geology Review*, *57*(13), 1735–1754.

Diwu, C. R., Sun, Y., Zhang, C. L., & Wang, H. L. (2010). The disintegration of Kuanping Group in North Qinling orogenic belts and neo-proterozoic N-MORB. *Acta Petrologica Sinica*, *26*(7), 2025–2038.

Diwu, C. R., Sun, Y., Zhao, Y., Liu, B. X., & Lai, S. (2014). Geochronological, geochemical, and Nd-hf isotopic studies of the Qinling complex, Central China: Implications for the evolutionary history of the north Qinling Orogenic Belt. *Geoscience Frontiers*, *5*(4), 499–513. https://doi.org/10.1016/j.gsf.2014.04.001

Dong, Y. P., Liu, X. M., Neubauer, F., Zhang, G. W., Tao, N., Zhang, Y. G., Zhang, X. N., & Li, W. (2013). Timing of Paleozoic amalgamation between the North China and South China blocks: Evidence from detrital zircon U–pb ages. *Tectonophysics*, *586*, 173–191.

Dong, Y. P., Liu, X. M., Zhang, G. W., Chen, Q., Zhang, X. N., Li, W., & Yang, C. (2012). Triassic diorites and granitoids in the Foping area: Constraint on the conversion from subduction to collision in the Qinling orogen, China. *Journal of Asian Earth Sciences*, *47*, 123–142.

Dong, Y. P., Zhang, G. W., Hauzenberger, C., Neubauer, F., Yang, Z., & Liu, X. M. (2011). Paleozoic tectonics and evolutionary history of the Qinling orogen: Evidence from geochemistry and

geochronology of ophiolite and related volcanic rocks. *Lithos*, *122*, 39–56.

Duan, L., Meng, Q. R., Zhang, C. L., & Liu, X. M. (2011). Tracing the position of the South China block in Gondwana: U–pb ages and hf isotopes of Devonian detrital zircons. *Gondwana Research*, *19*, 141–149.

Dupont-Nivet, G., Butler, R. F., Yin, A., & Chen, X. (2002). Paleomagnetism indicates no Neogene rotation of the Qaidam basin in North Tibet during Indo-Asian collision. *Geology*, *30*(3), 263–266.

Enkelmann, E., Weislogel, A. L., Ratschbacher, L., Eide, E., Renno, A., & Wooden, J. (2007). How was the Triassic Songpan-Ganzi basin filled? A provenance study. *Tectonics*, *26*, TC4007. https://doi.org/10.1029/2006TC002078

Gehrels, G., Kapp, P., DeCelles, P., Pullen, A., Blakey, R., Weislogel, A., Ding, L., Guynn, J., Martin, A., McQuarrie, N., & Yin, A. (2011). Detrital zircon geochronology of pre-tertiary strata in the Tibetan-Himalayan orogeny. *Tectonics*, *30*, TC5016. https://doi.org/10.1029/2011TC002868

Gehrels, G., Yin, A., & Wang, X. F. (2003). Detrital-zircon geochronology of the northeastern Tibetan plateau. *Geological Society of America Bulletin*, *115*, 881–896.

Gong, H. J., Zhu, L. M., Sun, B. Y., Li, B., & Guo, B. (2009). Zircon U-pb ages and hf isotope characteristics and their geological significance of the Shahewan, Caoping and Zhashui granitic plutons in the south Qinling orogeny (in Chinese with English abstract). *Acta Petrologica Sinica*, *25*, 248–264.

Hacker, B. R., Wallis, S. R., Ratschbacher, L., Grove, M., & Gehrels, G. (2006). High-temperature geochronology constraints on the tectonic history and architecture of the ultrahigh-pressure Dabie-Sulu orogeny. *Tectonics*, *25*, TC5006. https://doi.org/10.1029/2005TC001937

Halim, N., Cogné, J. P., Chen, Y., Atasiesi, R., Besse, J., Courtillot, V., Gilder, S., Marcoux, J., & Zhao, R. L. (1998). New cretaceous and early tertiary paleomagnetic results from Xining-Lanzhou basin, Kunlun and Qiangtang blocks, China: Implications on the geodynamic evolution of Asia. *Journal of Geophysical Research*, *103*, 21025–21045.

He, D. F., Dong, Y. P., Liu, X. M., Zhou, X. H., Zhang, F. F., & Sun, S. S. (2018). Zircon U–pb geochronology and hf isotope of granitoids in east Kunlun: Implications for the Neoproterozoic magmatism of Qaidam block, northern Tibetan plateau. *Precambrian Research*, *314*, 377–393.

He, D. F., Dong, Y. P., Liu, X. P., Yang, Z., Sun, S. S., Cheng, B., & Li, W. (2016). Tectono-thermal events in east Kunlun, northern Tibetan plateau: Evidence from zircon U–pb geochronology. *Gondwana Research*, *30*, 179–190.

He, S. P., Li, R. S., Wang, C., Zhang, H. F., Ji, W. H., Yu, P. S., Gu, P. Y., & Shi, C. (2011). Discovery of ca. 4.0 Ga detrital zircons in the Changdu block, north Qiangtang, Tibetan plateau. *Chinese Science Bulletin*, *56*(7), 647–658. https://doi.org/10.1007/s11434-010-4320-z

Hu, B., Zhai, M. G., Guo, J. H., Peng, P., Liu, F., & Liu, S. (2009). LA-ICP-MS U-pb geochronology of detrital zircons fromthe Huade group in the northern margin of the North China craton and its tectonic significance (in Chinese with English abstract). *Acta Petrologica Sinica*, *25*, 193–211.

Hubert, J. F. (1962). A zircon-tourmaline-rutile maturity index and the interdependence of the composition of heavy mineral assemblages with the gross composition and texture of sandstones. *Journal of Sedimentary Petrology*, *32*, 440–450.

Jian, X., Weislogel, A., & Pullen, A. (2019). Triassic sedimentary filling and closure of the eastern paleo-Tethys Ocean: New insights from detrital zircon geochronology of Songpan-Ganzi, Yidun, and west Qinling flysch in eastern Tibet. *Tectonics*, *38*, 767–787. https://doi.org/10.1029/2018TC005300

Jian, X., Weislogel, A., Pullen, A., & Shang, F. (2020). Formation and evolution of the eastern Kunlun range, northern Tibet: Evidence from detrital zircon U-pb geochronology and hf isotopes. *Gondwana Research*, *83*, 63–79.

Jiang, S. H., Nie, F. J., Fang, D. H., & Liu, Y. F. (2009). Geochronology and geochemical features of the main intrusive rocks in the Weishancheng area, Tongbai County, Henan (in Chinese with English abstract). *Acta Geologica Sinica*, *83*, 1011–1029.

Jiang, Y. H., Jin, G. D., Liao, S. Y., Zhou, Q., & Zhao, P. (2010). Geochemical and Sr-Nd-hf isotopic constraints on the origin of late Triassic granitoids from the Qinling orogen, Central China: Implications for a continental arc to continent-continent collision. *Lithos*, *117*, 183–197.

Jin, W. J., Zhang, Q., He, D. F., & Jia, X. Q. (2005). SHRIMP dating of adakites in western Qinling and their implications (in Chinese with English abstract). *Acta Petrologica Sinica*, *21*, 959–966.

Leng, C. B., Zhang, X. C., Hu, R. Z., Wang, S. X., Zhong, H., Wang, W. Q., & Bi, X. W. (2012). Zircon U–pb and molybdenite re–Os geochronology and Sr–Nd–pb–hf isotopic constraints on the genesis of the Xuejiping porphyry copper deposit in Zhongdian, Northwest Yunnan, China. *Journal of Asian Earth Sciences*, *60*, 31–48.

Lerch, M. F., Xue, F., & Kroner, A. (1995). A Paleozoic magmatic arc in the Heihe area, Qinling orogenic belt, Central China (in Chinese with English abstract). *Journal of Geology*, *103*, 437–449.

Li, R. B., Pei, X. Z., Li, Z. C., Pei, L., Liu, C. J., Chen, Y. X., Chen, G. C., Liu, Z. Q., & Yang, J. (2015). Geochemistry and zircon U–pb geochronology of granitic rocks in the Buqingshan tectonic mélange belt, northern Tibet plateau, China and its implications for Prototethyan evolution. *Journal of Asian Earth Sciences*, *105*, 374–389.

Li, R. B., Pei, X. Z., Li, Z. C., Sun, Y., Pei, L., Chen, G. C., Chen, Y. X., Liu, C. J., & Wei, F. H. (2013). Regional tectonic transformation in east Kunlun orogenic belt in early Paleozoic: Constraints from the geochronology and geochemistry of Helegangnaren alkali-feldspar granite. *Acta Geologica Sinica (English Edition)*, *87*(2), 333–345.

Li, R. B., Pei, X. Z., Pei, L., Li, Z. C., Chen, G. C., Chen, Y. X., Liu, C. J., & Wang, M. (2018). The early Triassic Andean-type Halagatu granitoids pluton in the east Kunlun orogen, northern Tibet plateau: Response to the northward subduction of the paleo-Tethys Ocean. *Gondwana Research*, *62*, 212–226.

Ling, W. L., Duan, R. C., Liu, X. M., Cheng, J. P., Mao, X. W., Peng, L. H., Liu, Z. X., Yang, H. M., & Ren, B. F. (2010). U-pb dating of detrital zircons from the Wudangshan Group in the South Qinling and its geological significance. *Chinese Science Bulletin*, *55*, 2440–2448. https://doi.org/10.1007/s11434-010-3095-6

Liou, J. G., Hacker, B. R., & Zhang, R. Y. (2000). Ultrahigh-pressure (UHP) metamorphism in the forbidden zone. *Science*, *287*, 1215–1216.

Liu, J. B., & Zhang, L. M. (2013). Neoproterozoic low to negative δ18O volcanic and intrusive rocks in the Qinling Mountains and their geological significance. *Precambrian Research*, *230*, 138–167.

Liu, S. W., Wang, Z. Q., Yan, Q. R., Li, Q. G., Zhang, D. H., Wang, J. G., Yang, B., Gu, L. B., & Zhao, F. S. (2006). Indosinian tectonic

setting of the southern Yidun arc: Constraints from SHRIMP zircon chronology and geochemistry of Dioritic porphyries and granites. *Acta Geologica Sinica*, *80*(3), 387–399.

Liu, X. M., Gao, S., Diwu, C. R., & Ling, W. L. (2008). Precambrian crustal growth of Yangtze craton as revealed by detrital zircon studies. *American Journal of Science*, *308*(4), 421–468. https://doi.org/10.2475/04.2008.02

Lu, S. N., Chen, Z. H., Xiang, Z. Q., Li, H. K., Li, H. M., & Song, B. (2006). U-pb ages of detrital zircons from the para-metamorphic rocks of the Qinling group and their geological significance (in Chinese with English abstract). *Earth Science Frontiers*, *13*(6), 303–310.

Lu, S. N., Li, H. K., Chen, Z. H., Hao, G. J., Zhou, H. Y., Guo, J. J., Niu, G. H., & Xiang, Z. Q. (2003). *Meso-neoproterozoic geological evolution of the Qinling and its respondence to Rodinia event (in Chinese)*. Geological Publishing House.

Matte, P., Tapponnier, P., Arnaud, N., Bourjot, L., Avouac, J. P., Vidal, P., Liu, Q., Pan, Y., & Wang, Y. (1996). Tectonics of Western Tibet, between the Tarim and the Indus. *Earth and Planetary Science Letters*, *142*, 311–330.

Meng, F. C., Jia, L. H., Ren, Y. F., Liu, Q., & Duan, X. P. (2017). Magmatic and metamorphic events recorded in the gneisses of the Wenquan region, east Kunlun Mountains, Northwest China: Evidence from the zircon U-pb geochronology. *Acta Petrologica Sinica*, *33*, 3691–3709.

Morton, A., & Hurst, A. (1995). Correlation of sandstones using heavy minerals: An example from the Statfjord formation of the snorre field, northern North Sea. In R. E. Dunay & E. A. Hailwood (Eds.), *Non-biostratigraphical methods of dating and correlation* (pp. 3–22). Geological Society Special Publication No. 89.

Nie, S., Yin, A., Rowley, D. B., & Jin, Y. (1994). Exhumation of the Dabie Shan ultra-high-pressure rocks and accumulation of the Songpan-Ganzi flysch sequence, Central China. *Geology*, *22*, 999–1002.

Pan, G., Ding, J., Yao, D., & Wang, L. (2004). *Geologic map of Qinghai-Xizang (Tibet) plateau and adjacent areas, scale 1:1,500,000*. Chengdu Cartographic Publishing House.

Pei, X. Z., Ding, S. P., Li, Z. C., Liu, Z. Q., Li, G. Y., Li, R. B., Wang, F., & Li, F. J. (2007). LA-ICP-MS zircon U-pb dating of the gabbro from the Guanzizhen ophiolite in the northern margin of the Western Qinling and its geological significance (in Chinese with English abstract). *Acta Geologica Sinica*, *81*(6), 772–786.

Pei, X. Z., Ding, S. P., Zhang, G. W., Liu, H. B., Li, Z. C., Li, G. Y., Liu, Z. Q., & Meng, Y. (2007). The LA-ICP-MS zircons U-pb ages and geochemistry of the Baihua basic igneous complexes in Tianshui area of west Qinling. *Science in China (Series D)*, *50*, 264–276.

Peng, T. P., Zhao, G. C., Fan, W. M., Peng, B. X., & Mao, Y. S. (2014). Zircon geochronology and hf isotopes of Mesozoic intrusive rocks from the Yidun terrane, eastern Tibetan plateau: Petrogenesis and their bearings with cu mineralization. *Journal of Asian Earth Sciences*, *80*, 18–33.

Pullen, A., Kapp, P., Gehrels, G., & Vervoort, J. D. (2008). Triassic continental subduction in Central Tibet and Mediterranean-style closure of the Paleotethys Ocean. *Geology*, *36*, 351–354.

Pullen, A., Kapp, P., Gehrels, G. E., Ding, L., & Zhang, Q. H. (2011). Metamorphic rocks in Central Tibet: Lateral variations and implications for crustal structure. *Geological Society of America Bulletin*, *123*(3–4), 585–600. https://doi.org/10.1130/B30154.1

Qi, S. S. (2015). *Petrotectonic assemblages and tectonic evolution of the east Kunlun orogenic belt in Qinghai Province* [PhD dissertation]. China University of Geosciences.

Qin, J. F., Lai, S. C., Grapes, R., Diwu, C. R., Ju, Y. J., & Li, Y. J. (2009). Geochemical evidence for origin of magma mixing for the Triassic monzonitic granite and its enclaves at Mishuling in the Qinling orogen (Central China). *Lithos*, *112*, 259–276.

Qin, J. F., Lai, S. C., & Li, Y. J. (2008). Slab breakoff model for the triassic post-collisional adakitic granitoids in the Qinling orogen, Central China: Zircon U-pb ages, geochemistry, and Sr-Nd-pb isotopic constraints. *International Geology Review*, *50*, 1080–1104.

Qin, J. F., Lai, S. C., Wang, J., & Li, Y. F. (2007). High-mg# adakitic tonalite from the Xichahe area, south Qinling orogenic belt (Central China): Petrogenesis and geological implications. *International Geology Review*, *49*, 1145–1158.

Ratschbacher, L., Franz, L., Enkelmann, E., Jonckheere, R., Porschke, A., Hacker, B. R., Dong, S. W., & Zhang, Y. Q. (2006). The Sino-Korean-Yangtze suture, the Huwan detachment, and the Paleozoic-tertiary exhumation of (ultra) high-pressure rocks along the Tongbai-Xinxian-Dabie. In B. R. Hacker, W. C. McClelland, & J. G. Liou (Eds.), *Ultrahigh-pressure metamorphism: Deep continental subduction* (pp. 45–75). Geological Society of America Special Paper, 403.

Reid, A., Wilson, C. J. L., Shun, L., Pearson, N., & Belousova, E. (2007). Mesozoic plutons of the Yidun arc, SW China: U/pb geochronology and hf isotopic signature. *Ore Geology Reviews*, *31*, 88–106.

Roger, F., Jolivet, M., Cattin, R., & Malavieille, J. (2011). Mesozoic–Cenozoic tectonothermal evolution of the eastern part of the Tibetan plateau (Songpan-Garzê, Longmen Shan area): Insights from thermochronological data and simple thermal modeling. In R. Gloaguen & L. Ratschbacher (Eds.), *Growth and collapse of the Tibetan Plateau* (Vol. *353*, pp. 9–25). Geological Society.

Roger, F., Jolivet, M., & Malavieille, J. (2008). Tectonic evolution of the Triassic fold belts of Tibet. *Comptes Rendus Geosciences*, *340*(2–3), 180–189.

Roger, F., Jolivet, M., & Malavieille, J. (2010). The tectonic evolution of the Songpan-Ganzi (North Tibet) and adjacent areas from Proterozoic to present: A synthesis. *Journal of Asian Earth Sciences*, *39*, 254–269.

Roger, F., Malavieille, J., Leloup, P. H., Calassou, S., & Xu, Z. (2004). Timing of granite emplacement and cooling in the Songpan–Garze fold belt (eastern Tibetan plateau) with tectonic implications. *Journal of Asian Earth Sciences*, *22*, 465–481.

Sengör, A. M. C. (1984). The Cimmeride orogenic system and the tectonics of Eurasia. *Geological Society of America*, *195*, 1–76.

Shao, F. L., Niu, Y. L., Liu, Y., Chen, S., Kong, J. J., & Duan, M. (2017). Petrogenesis of Triassic granitoids in the east Kunlun Orogenic Belt, northern Tibetan plateau and their tectonic implications. *Lithos*, *282*, 33–44.

Shao, T. B., Cheng, N. F., & Song, M. S. (2016). Provenance and tectonic-paleogeographic evolution: Constraints from detrital zircon U–pb ages of late Triassic-early Jurassic deposits in the northern Sichuan basin, Central China. *Journal of Asian Earth Sciences*, *127*, 12–31.

She, Z. B., Ma, C. Q., Mason, R., Li, J. W., Wang, G. C., & Lei, Y. H. (2006). Provenance of the Triassic Songpan-Ganzi flysch, West China. *Chemical Geology*, *231*, 159–175.

Shi, Y., Yu, J. H., & Santosh, M. (2013). Tectonic evolution of the Qinling orogenic belt, Central China: New evidence from geochemical, zircon U–pb geochronology and hf isotopes. *Precambrian Research*, *231*, 19–60.

Shi, Y., Yu, J. H., Xu, X. S., Qiu, J. S., & Chen, L. H. (2009). Geochronology and geochemistry of the Qinling group in the eastern Qinling orogen (in Chinese with English abstract). *Acta Petrologica Sinica*, *25*(10), 2651–2670.

Stampfli, G. M., & Borel, G. D. (2002). A plate tectonic model for the Paleozoic and Mesozoic. *Earth and Planetary Science Letters*, *196*, 17–33.

Su, B. R., Cui, X. Z., Tian, J. C., Lai, C. K., Ren, F., Ren, G. M., & Liu, S. L. (2019). *Detrital zircon provenance and palaeogeographic implications of the Ediacaran Shigu Group in the Zhongza Terrane, SW China*. International Geology Review. https://doi.org/10.1080/00206814.2019.1678201

Sun, W. D., Li, S. G., & Chen, Y. D. (2000). Zircon U-pb dating of granitoids from south Qinling, Central China and their geological significance. *Geochimica*, *29*, 209–216.

Sun, W. H., & Zhou, M. F. (2008). The ~860 Ma, cordilleran-type Guandaoshan Dioritic pluton in the Yangtze block, SW China: Implications for the origin of Neoproterozoic magmatism. *The Journal of Geology*, *116*, 238–253.

Sun, W. H., Zhou, M. F., Gao, J. F., Yang, Y. H., Zhao, X. F., & Zhao, J. H. (2009). Detrital zircon U–pb geochronological and Lu–hf isotopic constraints on the Precambrian magmatic and crustal evolution of the western Yangtze block, SW China. *Precambrian Research*, *172*, 99–126.

Sundell, K. E., & Saylor, J. E. (2017). Unmixing detrital geochronology age distributions. *Geochemistry, Geophysics, Geosystems*, *18*, 2872–2886.

Tang, Y., Zhang, Y. P., & Tong, L. L. (2017). Provenance of middle to late Triassic sedimentary rocks in the Zoige depression in the NE part of the Songpan–Ganzi Flysch Basin: Petrography, heavy minerals, and zircon U–pb geochronology. *Geological Journal*, *52*(S1), 449–462.

Tang, Y., Zhang, Y. P., & Tong, L. L. (2018). Mesozoic-Cenozoic evolution of the Zoige depression in the Songpan-Ganzi flysch basin, eastern Tibetan plateau: Constraints from detrital zircon U-pb ages and fission-track ages of the Triassic sedimentary sequence. *Journal of Asian Earth Sciences*, *151*, 285–300.

Tung, K. A., Yang, H. Y., Liu, D. Y., Zhang, J. X., Tseng, C. Y., & Wan, Y. S. (2007). SHRIMP U-pb geochronology of the detrital zircons from the Longshoushan group and its tectonic significance. *Chinese Science Bulletin*, *52*(10), 1414–1425.

Wan, Y. S., Liu, D. Y., Dong, C. Y., & Yin, X. Y. (2011). SHRIMP zircon dating of meta-sedimentary rock from the Qinling group in the north of Xixia, north Qinling Orogenic Belt: Constrains on complex histories of source region and timing of deposition and metamorphism (in Chinese with English abstract). *Acta Petrologica Sinica*, *27*(4), 1172–1178.

Wang, B. Q., Wang, W., Chen, W. T., Gao, J. F., Zhao, X. F., Yan, D. P., & Zhou, M. F. (2013). Constraints of detrital zircon U–pb ages and hf isotopes on the provenance of the Triassic Yidun group and tectonic evolution of the Yidun terrane, eastern Tibet. *Sedimentary Geology*, *289*, 74–98.

Wang, B. Q., Zhou, M. F., Li, J. W., & Yan, D. P. (2011). Late Triassic porphyritic intrusions and associated volcanic rocks from the Shangri-La region, Yidun terrane, eastern Tibetan plateau: Adakitic magmatism and porphyry copper mineralization. *Lithos*, *127*, 24–38.

Wang, J., Gou, G. N., Wang, Q., Zhang, C., Dan, W., Wyman, D. A., & Zhang, X. (2018). Petrogenesis of the late Triassic diorites in the Hoh Xil area, northern Tibet: Insights into the origin of the high-mg# andesitic signature of continental crust. *Lithos*, *300–301*, 348–360.

Wang, L. J., Griffin, W. L., Yu, J. H., & O'Reilly, S. Y. (2010). Precambrian crustal evolution of the Yangtze block tracked by detrital zircons from Neoproterozoic sedimentary rocks. *Precambrian Research*, *177*(1–2), 131–144. https://doi.org/10.1016/j.precamres.2009.11.008

Wang, L. J., Griffin, W. L., Yu, J. H., & O'Reilly, S. Y. (2013). U–pb and Lu–hf isotopes in detrital zircon from neoproterozoic sedimentary rocks in the northern Yangtze block: Implications for Precambrian crustal evolution. *Gondwana Research*, *23*, 1261–1272.

Wang, L. J., Yu, J. H., Griffin, W. L., & O'Reilly, S. Y. (2012). Early crustal evolution in the western Yangtze block: Evidence from U–pb and Lu–hf isotopes on detrital zircons from sedimentary rocks. *Gondwana Research*, *222–223*, 368–385.

Wang, L. Q., Pan, G. T., Ding, J., & Yao, D. S. (2013). *Geological map of the Tibetan plateau at a scale of 1:1.5 M with explanations (in Chinese)*. Geological Publishing House.

Wang, W., Li, F. L., & Bao, Z. Y. (2007). U-pb constraints on provenance and evolution of middle to late Triassic sediment in Songpan-Ganzi Basin (in Chinese with English abstract). *Geological Science and Technology Information*, *26*(5), 35–44.

Wang, X. L., Zhou, J. C., Griffin, W. L., Wang, R. C., Qiu, J. S., O'Reilly, S. Y., Xu, X. S., Liu, X. M., & Zhang, G. L. (2007). Detrital zircon geochronology of precambrian basement sequences in the Jiangnan orogen: Dating the assembly of the Yangtze and Cathaysia blocks. *Precambrian Research*, *159*, 117–131.

Wang, X. X., Wang, T., Castro, A., Pedreira, R., Lu, X. X., & Xiao, Q. H. (2011). Triassic granitoids of the Qinling orogen, Central China: Genetic relationship of enclaves and rapakivi-textured rocks. *Lithos*, *126*, 369–387.

Weislogel, A. L. (2008). Tectonostratigraphic and geochronologic constraints on evolution of the northeast paleotethys from the Songpan-Ganzi complex, Central China. *Tectonophysics*, *451*, 331–345.

Weislogel, A. L., Graham, S. A., Chang, E. Z., Wooden, J. L., & Gehrels, G. E. (2010). Detrital zircon provenance from three turbidite depocenters of the Middle–Upper Triassic Songpan-Ganzi complex, central China: Record of collisional tectonics, erosional exhumation, and sediment production. *Geological Society of America Bulletin*, *122*(11–12), 2041–2062.

Weislogel, A. L., Graham, S. A., Chang, E. Z., Wooden, J. L., Gehrels, G. E., & Yang, H. S. (2006). Detrital zircon provenance of the late Triassic Songpan-Ganzi complex: Sedimentary record of collision of the north and South China blocks. *Geology*, *34*, 97–100.

Wu, C., Yin, A., Zuza, A. V., Zhang, J. Y., Liu, W. C., & Ding, L. (2016). Pre-Cenozoic geologic history of the central and northern Tibetan plateau and the role of Wilson cycles in constructing the Tethyan orogenic system. *Lithosphere*, *8*(3), 254–292.

Xia, X. P., Sun, M., Zhao, G. C., & Luo, Y. (2006). LA-ICP-MS U–pb geochronology of detrital zircons from the Jining complex, North China craton and its tectonic significance. *Precambrian Research*, *144*, 199–212.

Xia, X. P., Sun, M., Zhao, G. C., Wu, F. Y., Xu, P., Zhang, J. H., & Luo, Y. (2006). U–pb and hf isotopic study of detrital zircons from the Wulashan khondalites: Constraints on the evolution of the Ordos terrane, Western block of the North China craton. *Earth and Planetary Science Letters*, *241*, 581–593.

Xiao, L., Zhang, H. F., Clemens, J. D., Wang, Q. W., Kan, Z. Z., Wang, K. M., Ni, P. Z., & Liu, X. M. (2007). Late Triassic granitoids of the eastern margin of the Tibetan plateau: Geochronology, petrogenesis and implications for tectonic evolution. *Lithos*, *96*, 436–452.

Xiong, F. H., Ma, C. Q., Chen, B., Ducea, M. N., Hou, M. C., & Ni, S. J. (2019). Intermediate-mafic dikes in the east Kunlun orogen, northern Tibetan plateau: A window into paleo-arc magma feeding system. *Lithos*, *340–341*, 152–165.

Xiong, F. H., Ma, C. Q., Jiang, H. A., Liu, B., Zhang, J. Y., & Zhou, Q. (2013). Petrogenetic and tectonic significance of Permian calc-alkaline lamprophyres, east Kunlun orogenic belt, Northern Qinghai-Tibet Plateau. *International Geology Review*, *55*(14), 1817–1834. https://doi.org/10.1080/00206814.2013.804683

Xiong, F. H., Ma, C. Q., Jiang, H. A., & Zhang, H. (2016). Geochronology and petrogenesis of Triassic high-K calc-alkaline granodiorites in the east Kunlun orogen, West China: Juvenile lower crustal melting during post-collisional extension. *Journal of Earth Science*, *27*(3), 474–490.

Xiong, F. H., Ma, C. Q., Wu, L., Jiang, H. A., & Liu, B. (2015). Geochemistry, zircon U-pb ages and Sr-Nd-hf isotopes of an Ordovician appinitic pluton in the east Kunlun orogen: New evidence for proto-Tethyan subduction. *Journal of Asian Earth Sciences*, *111*, 681–697.

Xiong, F. H., Ma, C. Q., Zhang, J. Y., Liu, B., & Jiang, H. A. (2014). Reworking of old continental lithosphere: An important crustal evolution mechanism in orogenic belts, as evidenced by Triassic I-type granitoids in the east Kunlun orogen, northern Tibetan plateau. *Journal of the Geological Society*, *171*, 847–863.

Xue, F., Kroner, A., Reischmann, T., & Lerch, M. F. (1996). Palaeozoic pre- and postcollision calc-alkaline magmatism in the Qinling orogenic belt, Central China, as documented by zircon ages on granitoid rocks. *Journal of the Geological Society*, *153*, 409–417.

Yan, Q. R., Chen, J. L., Wang, Z. Q., Yan, Z., Wang, T., Li, Q. G., Zhang, Z. Q., & Jiang, C. F. (2008). Zircon U-pb and geochemical analyses for leucocratic intrusive rocks in pillow lavas in the Danfeng group, north Qinling Mountains, China. *Science in China (Series D)*, *51*(2), 249–262.

Yan, Q. R., Wang, Z. Q., Chen, J. L., Yan, Z., Wang, T., Li, Q. G., Jiang, C. F., & Zhang, Z. Q. (2007). Tectonic setting and SHRIMP age of volcanic rocks in the Xieyuguan and Caotangou groups: Implications for the north Qinling Orogenic Belt (in Chinese with English abstract). *Acta Geologica Sinica*, *81*(4), 488–502.

Yan, Q. R., Wang, Z. Q., Hanson, A. D., Druschke, P. A., Yan, Z., Liu, D. Y., Jian, P., Song, B., Wang, T., & Jiang, C. F. (2003). SHRIMP age and geochemistry of the Bikou volcanic terrane: Implications for Neoproterozoic tectonics on the northern margin of the Yangtze craton. *Acta Geologica Sinica*, *77*(4), 479–490.

Yan, Z. K., Tian, Y. T., Li, R., Vermeesch, P., Sun, X. L., Li, Y., Rittner, M., Carter, A., Shao, C. J., Huang, H., & Ji, X. T. (2018). Late Triassic tectonic inversion in the upper Yangtze Block: Insights from detrital zircon U–Pb geochronology from southwestern Sichuan Basin. *Basin Research*, *31*(1), 92–113. https://doi.org/10.1111/bre.12310

Yang, W. T., Yang, J. H., Wang, X. F., & Du, Y. S. (2014). Uplift-denudation history of the Qinling orogen: Constrained from the detrital-zircon U–pb geochronology. *Journal of Asian Earth Sciences*, *89*, 54–65.

Yang, Z. Y., Zhang, S. X., & Yang, J. D. (2000). *Chinese stratigraphy-Triassic system (in Chinese)* (pp. 1–139). Geological Publishing House.

Yin, A., & Harrison, M. (2000). Geologic evolution of the Himalayan-Tibetan orogeny. *Annual Review of Earth and Planetary Sciences*, *28*, 211–280.

Yin, A., & Nie, S. Y. (1993). An indentation model for the north and South China collision and the development of the tan-Lu and Honam fault systems, eastern China. *Tectonics*, *12*(4), 801–813.

Yin, A., & Nie, S. Y. (1996). 20 A phanerozoic palinspastic reconstruction of China and its neighboring regions. In *The tectonic evolution of Asia*. Cambridge University.

Yuan, C., Zhou, M. F., Sun, M., Zhao, Y., Wilde, S., Long, X., & Yan, D. (2010). Triassic granitoids in the eastern Songpan Ganzi Fold Belt, SW China: Magmatic response to geodynamics of the deep lithosphere. *Earth and Planetary Science Letters*, *290*, 481–492.

Zhang, H. F., Parrish, R., Zhang, L., Xu, W. C., Yuan, H. L., Gao, S., & Crowley, Q. G. (2007). A-type granite and adakitic magmatism association in Songpan-Garze fold belt, eastern Tibetan plateau: Implication for lithospheric delamination. *Lithos*, *97*, 323–335.

Zhang, H. F., Zhang, L., Harris, N., Jin, L. L., & Yuan, H. L. (2006). U–pb zircon ages, geochemical and isotopic compositions of granitoids in Songpan–Garze fold belt, eastern Tibetan plateau: Constraints on petrogenesis and tectonic evolution of the basement. *Contribution to Mineralogy and Petrology*, *152*, 75–88.

Zhang, J. Y., Ma, C. Q., Xiong, F. H., & Liu, B. (2012). Petrogenesis and tectonic significance of the late Permian–middle Triassic calc-alkaline granites in the Balong region, eastern Kunlun orogen. *China. Geological Magazine*, *149*(5), 892–908.

Zhang, L. Y., Ding, L., Pullen, A., Xu, Q., Liu, D. L., Cai, F. L., Yue, Y. H., Lai, Q. Z., Shi, R. D., Ducea, M. N., Kapp, P., & Chapman, A. (2014). Age and geochemistry of western Hoh-Xil-Songpan-Ganzi granitoids, northern Tibet: Implications for the Mesozoic closure of the paleo-Tethys Ocean. *Lithos*, *190*, 328–348.

Zhang, Y., Jia, D., Shen, L., Yin, H. W., Chen, Z. X., Li, H. B., Li, Z. G., & Sun, C. (2015). Provenance of detrital zircons in the late Triassic Sichuan foreland basin: Constraints on the evolution of the Qinling orogen and Longmen Shan thrust-fold belt in Central China. *International Geology Review*, *57*(14), 1806–1824. https://doi.org/10.1080/00206814.2015.1027967

Zhang, Y. X., Tang, X. C., Zhang, K. J., Zeng, L., & Gao, C. L. (2014). U–Pb and Lu–Hf isotope systematics of detrital zircons from the Songpan–Ganzi Triassic flysch, NE Tibetan Plateau: Implications for provenance and crustal growth. *International Geology Review*, *56* (1), 29–56. https://doi.org/10.1080/00206814.2013.818754

Zhang, Y. X., Zeng, L., Li, Z. W., Wang, C. S., Zhang, K. J., Yang, W. G., & Guo, T. L. (2015). Late Permian-Triassic siliciclastic provenance, palaeogeography, and crustal growth of the Songpan terrane, eastern Tibetan plateau: Evidence from U-pb ages, trace elements, and hf isotopes of detrital zircons. *International Geology Review*, *57*(2), 159–181.

Zhou, D., & Graham, S. A. (1996). The Songpan-Ganzi Triassic flysch complex of the west Qinling Shan as a remnant ocean basin. In

A. Yin, & T. M. Harrison (Eds.), *The Tectonic Evolution of Asia* (pp. 281–299). Cambridge University Press.

Zhou, H. Z., Zhang, D. H., Wei, J. H., Wang, D. Z., Santosh, M., Shi, W. J., Chen, J. J., & Zhao, X. (2020). Petrogenesis of late Triassic mafic enclaves and host granodiorite in the eastern Kunlun Orogenic Belt, China: Implications for the reworking of juvenile crust by delamination-induced asthenosphere upwelling. *Gondwana Research*, *84*, 52–70.

Zhu, M., Chen, H. L., Zhou, J., & Yang, S. F. (2017). Provenance change from the middle to late Triassic of the southwestern Sichuan basin, Southwest China: Constraints from the sedimentary record and its tectonic significance. *Tectonophysics*, *700–701*, 92–107.

Zhu, X. Y., Chen, F. K., Li, S. Q., Yang, Y. Z., Nie, H., Siebel, W., & Zhai, M. G. (2011). Crustal evolution of the north Qinling terrain of the Qinling orogen, China: Evidence from detrital zircon U–pb ages and hf isotopic composition. *Gondwana Research*, *20*(1), 194–204.

Zhu, X. Y., Chen, F. K., Nie, H., Siebel, W., Yang, Y. Z., Xue, Y. Y., & Zhai, M. G. (2014). Neoproterozoic tectonic evolution of south Qinling, China: Evidence from zircon ages and geochemistry of the Yaolinghe volcanic rocks. *Precambrian Research*, *245*, 115–130.

SUPPORTING INFORMATION

Additional supporting information can be found online in the Supporting Information section at the end of this article.

How to cite this article: Tang, Y., Yin, A., Xu, X., An, K., & Zhang, Y. (2023). Tectonic evolution of the Triassic Songpan-Ganzi basin as constrained by a synthesis of multi-proxy provenance data. *Basin Research*, *35*, 28–60. https://doi.org/10.1111/bre.12703